



Cite this: *New J. Chem.*, 2023, 47, 18359

The effect of resonance-assisted hydrogen bond on the second-order nonlinear optical properties of pyridine hydrazone photoswitches: a quantum chemistry investigation[†]

Douniazed Hannachi, ^{*ab} Noureddine Khelfaoui, ^a Meriem Zaidi, ^{ac} Diha Yahiaoui, ^a Salima Lakehal, ^d Christophe Morell ^e and Henry Chermette ^{*e}

The effect of hydrogen bonds on the NLO properties was not considered as essential, in particular in pyridine hydrazone systems. Yet, we show in the present study that a control of these photoswitches depends on the strength of hydrogen bonds. In this study, we investigate a selection of 18 *E/Z* pyridine hydrazone photoswitch molecules to explore the impact of resonance-assisted hydrogen bond (RAHB) on the NLO properties in the *E/Z* isomers. Using quantum calculations at the ω B97XD/6-311+g(d) level of theory, we determine various electronic parameters, reactivity descriptors, bond length alternation (BLA) values, nuclear independent chemical shift (NICS) aromaticity indices, QTAIM topology, energy of hydrogen bond (E_{HB}), RAHB, and linear and nonlinear optical properties for these molecules. The agreement between the quantum calculations and experimental spectra is illustrated through TD-DFT calculations, showing small deviations. Contrary to conventional expectations, our findings demonstrated that the delocalization strength of the electrons and NLO properties of the *Z* isomers are significantly enhanced by the presence of a resonance-assisted hydrogen bond. The *Z*-isomer exhibited a lower excited state energy, weaker energy gap, smaller BLA value, larger dipole moment variations for the first excited state, higher $\Phi_{E \rightarrow Z}$, and electron delocalization at the quasi-cycle closed (RAHB) compared to the *E*-isomer. Furthermore, we find that the hyperpolarizability value of the title photoswitches increases as the wavelength of the incident light decreases, *i.e.*, $\beta(695) > \beta(1064) > \beta(1340) > \beta(\infty)$, and the dispersion has less effect at $\lambda = 1064$ and 1340 nm. Additionally, we observe a strong relation between the photoisomerization quantum yield ($\Phi_{E \rightleftharpoons Z}$) and static hyperpolarizability (β) of the first and second isomer, where $\Phi_{E \rightleftharpoons Z}$ is proportional to β of the second isomer and inversely proportional to b of the first isomer. This inverse trend between static hyperpolarizability and photoisomerization quantum yields is attributed to the electron-withdrawing character of substituents on the Ar ring. Our research provides valuable insights into optimizing the 2nd-order NLO properties of pyridine hydrazone photoswitch molecules. By understanding the influence of hydrogen bonding on the delocalization strength of the electrons (RAHB) and the shape-dependent NLO performance, we gain the ability to design and synthesize novel photoswitch molecules with enhanced NLO characteristics.

Received 20th June 2023,
Accepted 4th September 2023

DOI: 10.1039/d3nj02848h

rsc.li/njc

^a Laboratoire d'Électrochimie, d'Ingénierie Moléculaire et de Catalyse Redox (LEIMCR), Département d'Enseignement de Base en Technologie, Faculté de Technologie, Université Ferhat Abbas, Sétif-1, Algeria.

E-mail: douniazed_hannachi@univ-setif.dz

^b Département de Chimie, Faculté des Sciences, Université Ferhat Abbas, Sétif-1, Algeria

^c Laboratoire de Chimie, Ingénierie Moléculaire et Nanostructures (LCIMN), Université Ferhat Abbas Sétif 1, Sétif 19000, Algeria

^d Institut des Sciences de la Terre et de l'Univers, Université de Batna-2, Algeria

^e Université de Lyon, Université Claude Bernard Lyon 1, Institut des Sciences Analytiques, UMR CNRS 5280, 69622 Villeurbanne Cedex, France.

E-mail: henry.chermette@univ-lyon1.fr

[†] Electronic supplementary information (ESI) available. See DOI: <https://doi.org/10.1039/d3nj02848h>

Introduction

Molecular photoswitches are defined as chemical compounds that can reversibly be transformed from one isomer into another one with light irradiation. The two isomers differ from each other in various chemical and physical properties, such as geometrical structure, absorption spectra, oxidation/reduction potentials, magnetic properties, dielectric constant, refractive index, and others.^{1,2} This kind of molecules provides an invaluable tool for a large variety of applications, such as in information storage and processing,³ photo-pharmacology,



photo-actuators, remote-controllable reactions, and controllable drug transport and release.^{4,5}

Nonlinear optics (NLO) is a branch of optics that deals with phenomena arising from light-induced changes in the optical properties of compounds (e.g., phase, frequency, amplitude, polarization, and path). NLO compounds are materials that exhibit nonlinear optical responses, such as second-harmonic generation (SHG), optical Kerr effect, and third-harmonic generation (THG). These compounds have a wide range of applications in different fields, such as optical communication, optical computing, optical memory, and all-optical signal processing.^{6–11} Photochromic compounds, such as stilbenes, azobenzenes,^{12–14} diarylethenes,¹⁵ spirobifluorophanes,¹⁶ and fulgides,^{4,17} have excellent nonlinear optical responses (high hyperpolarizability). The combination between these two properties (photochromic and nonlinear optical) empowers generations of switchable second-order NLO materials. These classes of materials are called optical switches and have very high applications in optoelectronic and photonic technologies, including molecular-scale memory devices with multiple storage and nondestructive reading capacity.¹⁸ It is important to note that the photoswitching of second-order NLO properties makes sense only when the photoisomer compounds are thermally stable.¹⁹ From the literature, the switching of NLO properties has been performed by specific procedures including protonation/deprotonation, oxidation/reduction, and photoisomerization.^{20–24} In our work, we used photoisomerization to switch the NLO properties.

Recently, Mravec and collaborators^{25–27} designed and synthesized an extended set of 13 pyridine/quinoline hydrazones photoswitches. This new class of hydrazone-based P-type photoswitches is switchable between two isomers *Z* and *E* (see Fig. 1) and shows excellent thermal stability of both isomers. The operational wavelengths of the pyridine hydrazone structural motif shifted toward the visible region without the accompanying loss of their high thermal stability, and hydrazone *Z* retains good thermal stability.²⁵ Furthermore, the quantum-chemical calculations at the ω B97XD/def2-TZVPP level revealed a three-step inversion-rotation reaction mechanism of the thermal *E*-to-*Z* isomer. For benzoylpyridine hydrazones 1–8, 10, and 16, *E*-to-*Z* photoisomerization is more efficient compared to the *Z*-to-*E* process. From the work of Mravec *et al.*,²⁵ we can note that these compounds could be used for short-lived and long-lived information storage,²⁸ and these isomers could be utilized as photoswitch molecules.

In our work, we studied a series of 18 pyridine hydrazone photoswitches (*Zi* and *Ei* isomers, *i* = 1–18, see Fig. 1), which is divided in two subgroups, namely, one group of ten *Zi* and *Ei* isomers (where *i* = 1–8, 10, and 16) synthesized by Mravec *et al.*²⁵ and another one we designed, consisting of eight compounds (*i* = 9, 11–15, and 17–18 of *Ei* and *Zi* isomers), to investigate the substitutional effect on the hydrazine and ketone parts on the structural, electronic, reactivity, optical properties, and nonlinear responses. On ring 2, we chose two electron-withdrawing (EW) namely NO_2 and CN in order to study the effect of the EW character on electronic and optical properties. The main objective of this work is to show how the

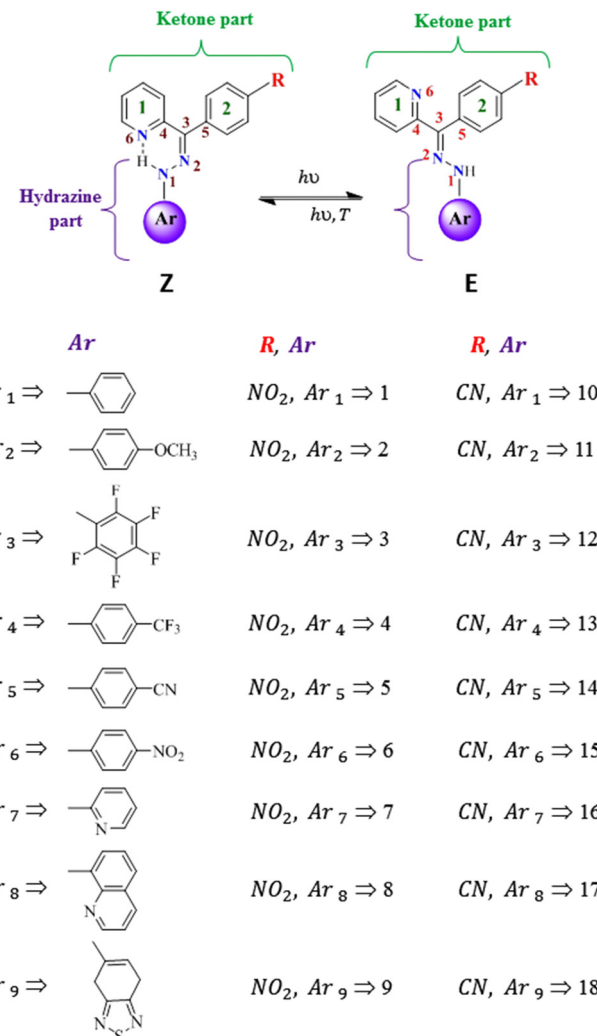


Fig. 1 Chemical structures of the pyridine hydrazones photoswitches (from ref. 25 for *i* = 1–8, 10, and 16).

hydrogen bond can enhance the NLO properties of the pyridine hydrazones photoswitches and try to find a relation between photoisomerization direction ($E \rightleftharpoons Z$) and hyperpolarizability.

The present paper is organized as follows. In Section 1, all computational details in the corresponding section and definitions are given; in Section 2, the quantum theory of atom-in-molecules (QTAIM) is analyzed; in Section 3, the bond length alternation (BLA) is presented; in Section 4, the NICS aromaticity indices are evaluated; in Section 5, the resonance-assisted hydrogen bond are given; in Section 6, the global reactivity descriptors are studied; in Section 7, the absorption spectra are discussed; and in Section 8, the static and dynamic NLO responses of *E* and *Z* isomers are calculated; the paper ends with some concluding remarks.

Computational details

The geometries of the *E* and *Z* isomers were fully optimized using the ω B97XD density functional^{29,30} with 6-311+g(d) basis



set.^{31,32} The ω B97XD is a range-separated hybrid exchange-correlation functional that includes damped atom-atom dispersion corrections.^{29,33} Quantum chemistry calculations were performed with Gaussian 09 program with TIGHT SCF convergence and ultra-fine integration grid.³⁴⁻³⁶ No symmetry constraints were applied and the local minima were confirmed on the potential energy surface by harmonic frequency calculations of the ground state for *E* and *Z* isomers at the same level. All the calculations were performed in the gas phase.

Chemical reactivity descriptors such as chemical hardness (η), electronic chemical potential (μ), and electronegativity (χ) can be evaluated from the frontier orbital energies HOMO and LUMO (ε_H and ε_L , respectively) using the following equation.³⁷

$$\mu = \frac{1}{2}(\varepsilon_H + \varepsilon_L) = -\chi \quad (1)$$

$$\eta = \varepsilon_L - \varepsilon_H \quad (2)$$

The chemical hardness (η) measures the stability of a molecule in terms of resistance to electron transfer, and the chemical potential (μ) characterizes the escaping tendency of electrons from the equilibrium system. The global electrophilicity index (ω), introduced by Parr *et al.*,³⁸ is calculated from the hardness and chemical potential.

$$\omega = \frac{\mu^2}{2\eta} \quad (3)$$

This index expresses the ability of a molecule to accept electrons from the environment.

Time-dependent density functional theory (TD-DFT) calculations were carried out at the same level of theory to evaluate the absorption wavelengths (λ) and corresponding oscillator strengths (f_{osc}) of electronic transitions. For TD-DFT calculations, sixty excited states were calculated.

Following the procedure proposed by LeBahers *et al.*,³⁹ the excited states of interest were examined using charge-transfer indices (CT) including charge-transfer distance (d^{CT}), transferred charge (q^{CT}), and the variation in dipole moment between the ground and the excited states ($\Delta\mu_{0 \rightarrow n} = q^{CT} \times d^{CT}$). In our work, the CT indices have been examined with MULTWLF program.⁴⁰

The electron density difference maps (EDDM) corresponding to the crucial excited states can be exactly evaluated as follows.

$$\Delta\rho(r) = \rho_{ex}(r) - \rho_{GS}(r) \quad (4)$$

$\rho_{ex}(r)$ and $\rho_{GS}(r)$ are defined as the electronic densities associated with the excited and ground states, respectively.

On the other hand, isotropic polarizability (α), polarizability density (ρ), and first hyperpolarizability (β_0) were calculated using analytical derivatives of the system energy (coupled-perturbed Kohn-Sham method)⁴¹ at the ω B97XD/6-311+g(d) level of theory. These parameters are defined as follows.^{8,42}

$$\alpha = \frac{1}{3}(\alpha_{xx} + \alpha_{yy} + \alpha_{zz}) \quad (5)$$

$$\rho = \frac{\langle \alpha \rangle}{V} \quad (6)$$

$$\langle \beta \rangle = \sqrt{\beta_x^2 + \beta_y^2 + \beta_z^2} \quad (7)$$

In this work, we also analyzed the second-harmonic generation ($\beta_{SHG}(-2\omega; \omega, \omega)$), electro-optical Pockels effect ($\beta(-\omega; \omega, 0)$), Hyper-Rayleigh scattering responses (β_{HRS}), and depolarization ratios (DR)^{8,43,44} at selected three frequencies (ω). Among these, two laser frequencies 0.0340 a.u. (1340 nm) and 0.0428 a.u. (1064 nm) are fed into these isomers. The frequency 0.0656 a.u. (695 nm) has also been imposed on these isomers. At the dynamic regime, the components of β_i are represented as follows.

For the second harmonic generation

$$\beta_i = \beta_{iii}(-2\omega; \omega, \omega) + \beta_{ijj}(-2\omega; \omega, \omega) + \beta_{ikk}(-2\omega; \omega, \omega) \quad (8)$$

In the case of electro-optical Pockels effect the is β_i obtained as follows.

$$\beta_i = \beta_{iii}(-\omega; \omega, 0) + \beta_{ijj}(-\omega; \omega, 0) + \beta_{ikk}(-\omega; \omega, 0) \quad (9)$$

The second-order NLO response β_{HRS} is given by⁴⁴

$$\langle \beta_{HRS} \rangle = \sqrt{\langle \beta_{ZZZ}^2 \rangle + \langle \beta_{XZZ}^2 \rangle} \quad (10)$$

where $\langle \beta_{ZZZ}^2 \rangle$ and $\langle \beta_{XZZ}^2 \rangle$ are the orientational averages of the β tensor without assuming Kleinman's conditions. Furthermore, β is typically decomposed into the sum of dipolar ($J = 1$) and octupolar ($J = 3$) tensorial components.⁴⁵

$$\langle \beta_{ZZZ}^2 \rangle = \frac{9}{45} |\beta_{J=1}|^2 + \frac{6}{105} |\beta_{J=3}|^2 \quad (11)$$

$$\langle \beta_{XZZ}^2 \rangle = \frac{1}{45} |\beta_{J=1}|^2 + \frac{4}{105} |\beta_{J=3}|^2 \quad (12)$$

The depolarization ratios (DR) provide information about the shape of the geometry of the chromophore, the part of the compound responsible for the NLO response (for an ideal one-dimensional system DR = 5, for an octupolar molecule DR = 1.5).

$$DR = \frac{\langle \beta_{ZZZ}^2 \rangle}{\langle \beta_{XZZ}^2 \rangle} \quad (13)$$

Results and discussion

Topological study

The intramolecular H-bond is one of the most prominent features that could influence the stability of compounds.⁴⁶ In this paper, we use the quantum theory of atom-in-molecules (QTAIM) to examine this bond.^{47,48} In this theory, the critical points (in ring (RCP) or bond (BCP)) are the positions where the gradient is null and which can be classified according to the electron density (ρ) and its Laplacian ($\nabla^2(\rho)$), total electron energy density (H), kinetic electron energy density (G), and



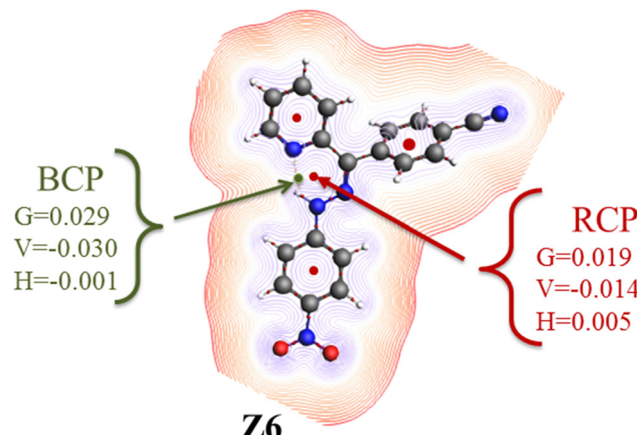


Fig. 2 Molecular topology of the Z6-isomer.

potential electron energy density (V).^{47,49} The QTAIM calculations were carried out for Z-isomers using the Amsterdam Density Functional (ADF18) program developed by Baerends *et al.*,^{50,51} and the results of the calculation are summarized in Table S1 (ESI†). Fig. 2 depicts the molecular graphs corresponding to the Z6 isomer, where the red circle indicates the ring critical point (RCPs) and the green circle indicates the bond critical point (BCPs).

In all of the Z-isomers, ring critical point (RCP: N1–N2–C3–C4–N6···H) and hydrogen bonds between the ketone and hydrazine moiety are observed (see Table S1, ESI† and Fig. 2). It is interesting to note that the formation of this RCP resulted from the cyclic nature of electron current and also confirms the existence of hydrogen bonding (N1–H···N6).

QTAIM analysis shows that the critical point at the hydrogen bond N1–H···N6 (BCP) has electronic density ranges from 0.012 to 0.015 a.u., while the Laplacian of the electron densities is in the range of 0.96–0.100 a.u., $G = 0.019$, $V = -0.014$, and $H = 0.005$ (with the exception of the isomers substituted with Ar₇ and Ar₈, where the H value amounts from -0.0005 to -0.0003 a.u.), whereas for the ring critical points (RCP: N1–N2–C3–C4–N6···H), the values electronic density is in the range of 0.031–0.035 and its Laplacian is in the range of 0.103 to 0.109; the values of G , V , and H are 0.028, -0.027 to -0.030 , and 0.05 a.u., respectively. From this value, we note that there is no effect of the substitutions (Ar moiety and EW groups (CN, NO₂) at the ring 2) on the H-bond and RCP (see Table S1, ESI†). On the other hand, H-bond exhibits positive values of $\nabla^2(\rho_{BCP})$ and negative values of H_{BCP} , which are typical of intermediate hydrogen bonds. Furthermore, in the RCP, we observe an increase in the kinetic energy (G) over the potential energy $|V|$, which means that the electrons are moving faster in ring N1–N2–C3–C4–N6···H or, in other words, the electrons are less localized. In the case of BCP H-bond (H···N6), we note that $G \leq |V|$, indicating that the electrons are localized in this region of Z-isomers.⁵²

On the other hand, BLA is a structural parameter, defined as the average difference between the lengths of a single bond and the adjacent multiple bonds in a π -delocalized

Table 1 Bond length alternation (BLA₁ and BLA₂, Å) for the *Ei* and *Zi* ($i = 1$ to 18) compounds

<i>Ei</i>	BLA ₁	BLA ₂	<i>Zi</i>	BLA ₁	BLA ₂	<i>Ei</i>	BLA ₁	BLA ₂	<i>Zi</i>	BLA ₁	BLA ₂
<i>E1</i>	0.120	0.126	<i>Z1</i>	0.104	0.107	<i>E10</i>	0.120	0.126	<i>Z10</i>	0.104	0.108
<i>E2</i>	0.119	0.125	<i>Z2</i>	0.099	0.103	<i>E11</i>	0.119	0.125	<i>Z11</i>	0.100	0.104
<i>E3</i>	0.140	0.143	<i>Z3</i>	0.125	0.125	<i>E12</i>	0.141	0.144	<i>Z12</i>	0.113	0.114
<i>E4</i>	0.125	0.130	<i>Z4</i>	0.111	0.114	<i>E13</i>	0.125	0.130	<i>Z13</i>	0.111	0.114
<i>E5</i>	0.126	0.132	<i>Z5</i>	0.113	0.116	<i>E14</i>	0.127	0.132	<i>Z14</i>	0.114	0.117
<i>E6</i>	0.128	0.132	<i>Z6</i>	0.115	0.118	<i>E15</i>	0.128	0.133	<i>Z15</i>	0.116	0.118
<i>E7</i>	0.124	0.128	<i>Z7</i>	0.110	0.113	<i>E16</i>	0.123	0.128	<i>Z16</i>	0.111	0.113
<i>E8</i>	0.121	0.126	<i>Z8</i>	0.108	0.110	<i>E17</i>	0.122	0.126	<i>Z17</i>	0.110	0.112
<i>E9</i>	0.125	0.130	<i>Z9</i>	0.111	0.113	<i>E18</i>	0.125	0.131	<i>Z18</i>	0.112	0.114

$$\text{BLA}_1 = 1/2(d_{1-2} + d_{3-4} - 2d_{2-3}), \text{BLA}_2 = 1/2(d_{1-2} + d_{3-5} - 2d_{2-3}).$$

isomer. For the title isomers, we calculated the BLAs (BLA₁ and BLA₂, see atom numbering in Fig. 1) and summarized them in Table 1.

The DFT calculation shows that in the whole set of isomers (Z and E), the BLA₁ is smaller than the BLA₂, which may be ascribed to the donation effect of the pyridine ring (ring 1, see Fig. 1). When comparing E1–E9 isomers to E10–E18, it is found that the BLA₁ and BLA₂ values of *Ei*-isomers substituted by NO₂ group are similar to that of the *Ei*-isomers substituted by the CN group. For example, BLA₁ = 0.128 and BLA₂ = 0.132 Å for E6 and E16, respectively. We observed the same results for the Z-isomers, with the exception of Z3 and Z12 compounds, where the values are different (BLA₁(Z3) = 0.125 ≠ BLA₁(Z12) = 0.113 and BLA₁(Z3) = 0.125 ≠ BLA₂(Z12) = 0.114). From these results, we can conclude that the substitution of a NO₂ by a CN group in the R position does not introduce significant changes in the bond length alternation BLA₁ and BLA₂ along the conjugated linker, which connects the Ar and ketone parts. On the other hand, we observe that the BLA₁₋₂ values of the Z1–Z18 isomers are smaller than that of the corresponding E1–E18 isomers. This suggests that the π -conjugation of the Z-isomers is stronger than that of the corresponding E-isomers, which is certainly related to the existence of the hydrogen bond N1–H···N6 (stronger electrostatic effects in the Z-isomers). In addition, the smallest BLA₁₋₂ values are obtained when Ar is the C₆H₄-p-OCH₃ (Ar₂) group (isomers Z2, Z11, and E2, E11), whereas the largest values are obtained for Ar₃ = C₆F₆ (E3, E12, Z3, and Z12 isomers). Thus, the effect of the nature of the Ar group is stronger for the BLA₁ and BLA₂ values than the nature of the R substituent (NO₂ and CN). Generally, the BLA₁₋₂ values of Z1–Z9, Z10–18, E1–E9, and E10–18 isomers increase following the order: Ar₂ < Ar₁ < Ar₈ < Ar₇ < Ar₉ < Ar₄ < Ar₅ < Ar₆ < Ar₃. From this result, we can note that the BLA₁₋₂ values increase with the increase in the EW character of the substituents on the Ar-ring.

The calculated hydrogen bond angle and dihedral angle between the hydrazine part and rings 1 and 2 are listed in Table S2 (ESI†). Regardless of the nature of the R substituent, we observed that E to Z isomerization results in a decrease in the dihedral angle φ_1 by approximately 27°, while φ_2 deviates by 74°. On the other hand, for the Z isomers, it is found that the dihedral angle (φ_1) measured between ring 1 and the hydrazine



part is approximately 19° , which is smaller compared to the dihedral angle between ring 2 and the hydrazine part ($\varphi_2 = 44^\circ$). This decrease in angle (φ_1) enhances the π -electron conjugation between ring 1 and the hydrazine part more than that between ring 2 and the hydrazine part. Additionally, the presence of hydrogen bonds leads to reduced dihedral angles between the Ar-linker-ring 2 in the *Z*-isomer. This observation is reinforced by the slightly lower bond length alternation (BLA₂) values in the *Z*-isomer compared to the *E*-isomer.

On the other hand, for the *Z* isomers, the N1-H···N6 hydrogen bond angle (φ_3) has been observed to be 130° . However, an exception is noted in *Z7*, *Z8*, *Z16*, and *Z17*, where the angle φ_3 is measured at 127° (Table S2, ESI[†]). Notably, this angle aligns well with the IUPAC recommendations, which suggest that hydrogen bond angles should preferably be above 110° .⁵³

Aromaticity

The local aromaticity, nonaromaticity as well as anti-aromaticity in the title compounds is assessed by NICS calculations, which was introduced by von Rague Schleyer *et al.*^{54,55} The NICS was calculated at the ring center or cages and described as the negative value of the isotropic shielding constant.⁵⁶ Noted that the strongly negative NICS values (*i.e.*, magnetically shielded) denote the presence of induced diatropic ring currents and “aromaticity”, whereas the positive values (*i.e.*, deshielded) at the chosen point indicate paratropic ring current and “anti-aromaticity”.⁵⁷ In this work, we used the NICS_{ZZ}(1) index, which is calculated to be 1 Å above the center of the ring under consideration. The results of NICS_{ZZ}(1) calculation for all the isomers considered are listed in Table 2.

For both the isomers, the quantum calculation shows that the NICS_{ZZ}(1) index is more negative in rings 2 than in the ring 1.

Table 2 NICS_{ZZ} aromaticity index

NICS _{ZZ}			NICS _{ZZ}			NICS _{ZZ}			NICS _{ZZ}		
<i>E1</i>	1	-8.089	Z1	1	-9.396	<i>E10</i>	1	-8.120	Z10	1	-9.385
	2	-12.941		2	-10.109		2	-13.197		2	-10.709
	3	-9.693		3	-9.387		3	-9.520		3	-9.405
				QCC	27.197					QCC	27.227
<i>E2</i>	1	-8.160	Z2	1	-9.370	<i>E11</i>	1	-7.941	Z11	1	-9.275
	2	-13.098		2	-9.958		2	-12.942		2	-10.621
	3	-10.122		3	-8.630		3	-10.031		3	-8.600
				QCC	26.980					QCC	27.051
<i>E3</i>	1	-8.796	Z3	1	-10.370	<i>E12</i>	1	-8.802	Z12	1	-10.318
	2	-13.019		2	-10.217		2	-13.119		2	-10.527
	3	-15.667		3	-15.404		3	-15.846		3	-15.612
				QCC	27.127					QCC	27.027
<i>E4</i>	1	-8.406	Z4	1	-9.924	<i>E13</i>	1	-8.287	Z13	1	-9.827
	2	-13.065		2	-10.738		2	-13.843		2	-11.812
	3	-7.719		3	-7.657		3	-7.644		3	-7.566
				QCC	27.357					QCC	27.406
<i>E5</i>	1	-8.826	Z5	1	-10.058	<i>E14</i>	1	-8.482	Z14	1	-9.995
	2	-13.338		2	-10.960		2	-13.260		2	-11.221
	3	-7.479		3	-7.216		3	-7.364		3	-7.265
				QCC	27.323					QCC	27.358
<i>E6</i>	1	-8.798	Z6	1	-10.147	<i>E15</i>	1	-8.491	Z15	1	-9.987
	2	-13.193		2	-10.989		2	-13.217		2	-11.256
	3	-6.483		3	-6.090		3	-6.348		3	-6.267
				QCC	27.459					QCC	27.630
<i>E7</i>	1	-8.362	Z7	1	-9.875	<i>E16</i>	1	-8.324	Z16	1	-9.856
	2	-12.849		2	-10.303		2	-13.101		2	-10.786
	3	-6.512		3	-6.562		3	-6.335		3	-6.678
				QCC	26.969					QCC	27.113
<i>E8</i>	1	-7.902	Z8	1	-9.346	<i>E17</i>	1	-8.237	Z17	1	-9.230
	2	-12.916		2	-9.793		2	-12.893		2	-10.319
	3	-8.522		3	-8.596		3	-8.409		3	-8.293
	1'	-8.961		QCC	28.264		1'	-8.984		QCC	28.214
<i>E9</i>	1	-8.864	Z9	1	-9.902	<i>E18</i>	1	-8.388	Z18	1	-9.879
	2	-13.341		2	-10.205		2	-13.466		2	-10.747
	3	-0.342		3	-0.216		3	-0.288		3	-0.0602
	1'	-13.128		QCC	27.615		1'	-13.171		QCC	27.736
				1'	-14.047					1'	-12.639



The aromaticity in ring 2 substituted with NO_2 group is notably smaller than that substituted with the CN group (with the exception of isomers E2, E5, and E8). At the same time, the localization of NO_2 group at ring 2 results in increases in the anti-aromaticity of quasi-cycle closed, with exception for the 3 and 8 compounds. However, it leads to lower stability of these isomers (Z1 to Z9) in comparison with the isomers Z10 to Z18 (CN group at the ring 2). On the other hand, the $\text{NICS}_{\text{ZZ}}(1)$ results obtained for Ar-ring (ring 3) indicate that this ring is aromatic and less stable than the ring 2, with the exception of the compounds 3 and 12, where Ar_3 exhibits a high aromaticity diatropicity and stability. The order of the $\text{NICS}_{\text{ZZ}}(1)$ index of Ar-ring is $\text{Ar}_3 > \text{Ar}_2 > \text{Ar}_1 > \text{Ar}_8 > \text{Ar}_4 > \text{Ar}_5 > \text{Ar}_7 > \text{Ar}_6 > \text{Ar}_9$.

The $\text{NICS}_{\text{ZZ}}(1)$ indexes for Z isomers reveal a reduction in the aromatic behavior in rings 2 and Ar, whereas ring 1 shows an increase in the aromatic character in comparison with corresponding E isomers (Table 2). These variations in aromaticity between Z and E isomers can be attributed to the RAHB effect and pronounced anti-aromatic behavior in quasi-cycle closed in Z isomers. In general, we can conclude that the Z-isomer displays a smaller BLA value as well as larger aromatic character (ring 1) than that of the corresponding E-isomer.

Mravec *et al.* found that in the benzoylpyridine hydrazones 1–8, 10, and 16, the $E \rightarrow Z$ photoisomerization is more efficient compared to the $Z \rightarrow E$ process.²⁵ We can attribute these results to the Z-isomer shape, which features an anti-aromatic ring (quasi-cycle closed) surrounded by three aromatic rings (1, 2, and Ar ring).

Resonance-assisted hydrogen bond

Based on the analyzes of the data presented in Table 3, the E-isomers exhibit a chemical shift of the bridging hydrogen at the range of $\delta_{\text{N}_1\text{H},\text{E}} = 5.6\text{--}8.8$ ppm, and the $\text{N}_1\text{-H}$ stretching frequency in the range of $\sigma_{\text{N}_1\text{H},\text{E}} = 3553\text{--}3581 \text{ cm}^{-1}$. On the other hand, the Z isomers display significantly higher $\delta_{\text{N}_1\text{H}}$ ($\delta_{\text{N}_1\text{H},\text{Z}} = 11.7\text{--}13.5$ ppm) and lower $\sigma_{\text{N}_1\text{H}}$ values

($\sigma_{\text{N}_1\text{H},\text{Z}} = 3465\text{--}3508 \text{ cm}^{-1}$) compared to the corresponding E-isomer. The observed variations in Z isomers are a result of the presence of intramolecular $\text{N}_1\text{-H} \cdots \text{N}_6$ hydrogen bonding, leading to the formation of a quasi-ring structure $\text{N}_1\text{-N}_2\text{-C}_3\text{-C}_4\text{-N}_6\cdots\text{H}$ (the distance $\text{N}_1\text{-N}_6$ and $\text{H} \cdots \text{N}_6$ is ~ 2.691 and 1.922 \AA , respectively). According to the literature and our calculations, this quasi-ring structure is almost planar^{58–65} (see Table S2, ESI†) and distinguished by short $\text{N}_1\text{-N}_6$ distances and longer H-N_1 bonds ($r_{\text{H-N}_1,\text{Z}} \approx 1.018 \text{ \AA}$ and $r_{\text{H-N}_1,\text{E}} \approx 1.012 \text{ \AA}$). Furthermore, analysis using QTAIM indicates a delocalization of electrons within the quasi-cycle closed (RCP). Additionally, we observed lower $\delta_{\text{N}_1\text{H},\text{Z}}$ frequencies and down-field shift of the $\delta_{\text{N}_1\text{H},\text{Z}}$. These findings strongly support the resonance-assisted hydrogen bond model (RAHB) proposed by Gilli *et al.*,^{66–68} and we can conclude that this quasi-cycle closed (QCC) created an RAHB phenomenon.

We note that in the closed quasi-cycle of the Z isomer, the enhancement of conjugation results from the effective charge transfer occurring between the π -donor amine nitrogen to the pyridine nitrogen through the $\text{C}=\text{N}$ double bond. This charge transfer is notably more efficient compared to a similar transfer in the open quasi-cycle of the E isomer, where it is attributed to the formation of a RAHB system.

Numerous methods have emerged over time to estimate the energy of hydrogen bonds. Among these, the widely employed approach for estimating E_{HB} involves utilizing the relation established by Espinosa *et al.* According to their work, the potential electron energy density (V) at the BCP is directly proportional to the energy of the hydrogen bond (E_{HB}), with an angular coefficient of 0.5.⁶⁹ Despite its popularity, Espinosa's equation tends to yield a significantly overestimated energy of HB.^{70,71} More recently, Afonin *et al.* introduced a novel linear relationship between the calculated (V) and the energy (E) of hydrogen bonds.⁷² They achieved this utilizing empirical ^1H NMR data and represented it as "eqn (14)".

$$E_{\text{HB}}(V) = 0.277 \times |V| - 0.45 \quad (14)$$

Table 3 Summarizes of the $\delta_{\text{N}_1\text{H}}$ chemical shifts (ppm), $\sigma_{\text{N}_1\text{H}}$ stretching frequency (cm^{-1}), and the distance $r_{\text{N}_1\text{-H}}$ (\AA) for E_i and Z_i ($i = 1$ to 18) isomers. The energy of HB ($E_{\text{HB}}(V)$ kcal mol $^{-1}$) and distance ($r_{\text{H}\cdots\text{N}_6}$, $r_{\text{N}_1\text{-N}_6}$ \AA) for each Z isomers are also given

	$\delta_{\text{N}_1\text{H}}$	$\sigma_{\text{N}_1\text{H}}$	$r_{\text{N}_1\text{-H}}$		$\delta_{\text{N}_1\text{H}}$	$\sigma_{\text{N}_1\text{H}}$	$r_{\text{N}_1\text{-H}}$	$r_{\text{H}\cdots\text{N}_6}$	$r_{\text{N}_1\text{-N}_6}$	$E_{\text{HB}}(V)$
E1	6.32	3576.90	1.012	Z1	12.26	3500.52	1.016	1.921	2.695	4.59
E2	6.04	3578.16	1.012	Z2	12.21	3489.31	1.017	1.919	2.691	4.59
E3	5.62	3565.79	1.013	Z3	11.70	3465.57	1.018	1.913	2.682	4.59
E4	6.25	3579.79	1.012	Z4	12.25	3496.47	1.017	1.916	2.693	4.59
E5	6.11	3576.89	1.012	Z5	12.38	3500.48	1.017	1.913	2.690	4.76
E6	6.28	3578.79	1.012	Z6	12.43	3474.69	1.017	1.907	2.688	4.76
E7	7.00	3571.91	1.013	Z7	12.32	3506.80	1.017	1.956	2.700	4.06
E8	8.76	3555.43	1.014	Z8	13.58	3481.68	1.018	1.946	2.691	4.24
E9	5.98	3581.15	1.012	Z9	12.14	3486.62	1.016	1.915	2.692	4.59
E10	6.13	3577.43	1.012	Z10	12.36	3492.43	1.016	1.914	2.689	4.76
E11	6.22	3576.14	1.012	Z11	12.18	3489.44	1.016	1.917	2.692	4.59
E12	5.60	3562.77	1.014	Z12	11.49	3478.79	1.017	1.923	2.687	4.59
E13	6.28	3579.79	1.012	Z13	12.19	3496.47	1.017	1.916	2.693	4.76
E14	6.13	3576.36	1.012	Z14	12.28	3491.46	1.017	1.913	2.691	4.76
E15	6.23	3576.04	1.012	Z15	12.37	3496.83	1.017	1.909	2.688	4.76
E16	6.87	3576.35	1.013	Z16	12.40	3507.92	1.017	1.949	2.695	4.24
E17	8.78	3553.10	1.014	Z17	13.51	3482.99	1.018	1.949	2.693	4.24
E18	5.95	3580.07	1.012	Z18	12.20	3491.47	1.016	1.917	2.691	4.59



In order to assess the strength of the hydrogen bond, we employed eqn (14) and presented the corresponding calculation results in Table 3. The analysis demonstrates that the hydrogen bond energy in the *Z* isomers varies between 4.1 and 4.8 kcal mol⁻¹, placing them within the category of medium-strength hydrogen bonds.⁷² It is worth mentioning that the relatively weak energy of $E_{\text{HB}}(V)$ does not have a significant impact on the optical properties of photoswitches.

Reactivity

The values of global reactivity descriptors chemical potential (μ), hardness (η), and electrophilicity index (ω) calculated for each *Ei* and *Zi* isomers ($i = 1$ to 18) are collected and presented in Table 4 and Fig. 3.

From these results, we can see that the *E*-isomers show the largest values of the chemical hardness, which signifies a greater stability and lower reactivity, whereas the smallest value of hardness are observed for the corresponding *Z*-isomers; this observation is in line with the experimental results of Mravc *et al.*²⁵ The overall increasing order of hardness in the studied compounds is as follows: $E2 < E8 < E1 < E9 < E4 < E5 < E18 < E7 < E6 < E17 < E11 < E15 < E3 < E10 < E14 < E13 < E16 < E12$. The same order is observed for corresponding *Z*-isomers (see Fig. 3).

On the other hand, the potential chemistry of *Z*-isomers is larger than that of the corresponding *E*-isomer. These results indicate that the trend of the electrons to leave the equilibrium systems increases from *Z* to *E* isomers. In other words, the rise of the μ values indicates that the isomers with RAHB system have the greatest tendency to donate electrons.

The chemical potential values of *Ei* isomers increase in the following order.

$E3 < E6 < E5 < E4 < E15 < E9 < E12 < E7 < E18 < E14 < E1 < E2 < E13 < E8 < E16 < E10 < E17 < E11$

According to the global electrophilicity scale,^{56,73} the *Ei* and *Zi* isomers where $i = 1$ to 9 (with electron-withdrawing NO_2) and $i = 12, 14\text{--}15, 18$, and *Z13* can be classified as strong

Table 4 Chemical potential (μ , eV), chemical hardness (η , eV), and electrophilicity index (ω , eV) of the *Ei* and *Zi* ($i = 1$ to 18) compounds

	μ	η	ω		μ	η	ω
<i>E1</i>	-4.277	6.617	1.382	<i>Z1</i>	-4.163	6.574	1.318
<i>E2</i>	-4.230	6.536	1.369	<i>Z2</i>	-3.969	6.304	1.249
<i>E3</i>	-4.736	7.270	1.542	<i>Z3</i>	-4.596	7.057	1.497
<i>E4</i>	-4.550	6.863	1.509	<i>Z4</i>	-4.442	6.792	1.452
<i>E5</i>	-4.602	6.868	1.542	<i>Z5</i>	-4.511	6.768	1.503
<i>E6</i>	-4.706	6.968	1.589	<i>Z6</i>	-4.630	6.822	1.571
<i>E7</i>	-4.380	6.923	1.385	<i>Z7</i>	-4.314	6.764	1.376
<i>E8</i>	-4.116	6.549	1.293	<i>Z8</i>	-4.075	6.414	1.294
<i>E9</i>	-4.460	6.709	1.482	<i>Z9</i>	-4.400	6.548	1.478
<i>E10</i>	-3.881	7.335	1.027	<i>Z10</i>	-3.903	6.991	1.089
<i>E11</i>	-3.850	7.214	1.027	<i>Z11</i>	-3.692	6.758	1.009
<i>E12</i>	-4.410	7.888	1.233	<i>Z12</i>	-4.384	7.382	1.302
<i>E13</i>	-4.201	7.495	1.177	<i>Z13</i>	-4.233	7.111	1.269
<i>E14</i>	-4.292	7.421	1.241	<i>Z14</i>	-4.330	7.027	1.334
<i>E15</i>	-4.534	7.248	1.418	<i>Z15</i>	-4.509	6.966	1.459
<i>E16</i>	-4.031	7.544	1.077	<i>Z16</i>	-4.046	7.186	1.139
<i>E17</i>	-3.856	7.004	1.061	<i>Z17</i>	-3.854	6.757	1.099
<i>E18</i>	-4.340	6.892	1.366	<i>Z18</i>	-4.292	6.674	1.380

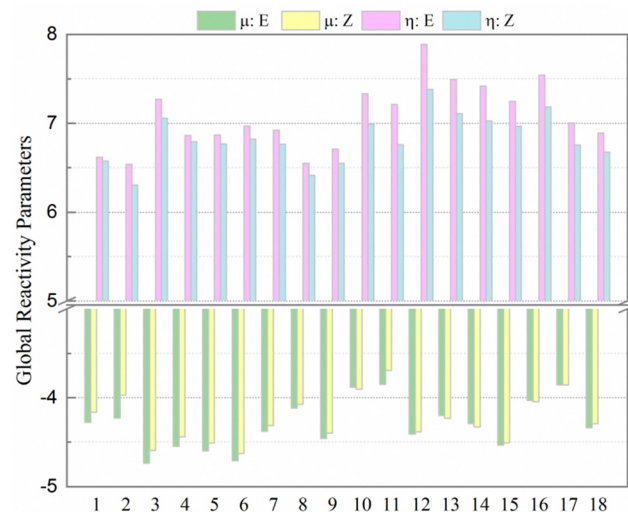


Fig. 3 Global reactivity indices of *Ei* and *Zi* ($i = 1$ to 18) isomers.

electrophiles (1.23 to 1.58 eV). Besides, the *Zi* and *Ei* isomers of $i = 10, 11, 16\text{--}17$, and *E13* (CN substituent) display a moderate electrophilicity (1.00 to 1.17 eV).

Linear optical properties

The calculated excited state transition energies (ΔE), wavelength (λ), oscillator strengths (f), charge transfer (q^{CT} , $|e|$), charge transfer distance (d^{CT} , Å), dipole moment variation ($\Delta\mu$, D), and major molecular orbital transitions of isomers are summarized in Table 5 and Table S3 (ESI[†]). Furthermore, the shapes of the MOs of specific excitation and EDDM for all isomers are provided in the ESI[†] (Fig. S1 and S2).

Theoretically, the electron transition energy is a decisive property of optical absorption because it is closely related to the position of the maximum absorption peak (λ_{Max}). From the simulated absorption spectra (Fig. S3, ESI[†]), we find that the maximum absorption wavelength (λ_{Max}) of the title compounds correspond to the first excited state $S_0 \rightarrow S_1$ in the range from 290 to 366 nm and presented a large oscillator strength value (with the exception of *E3*, which exhibits a very weak oscillator strength ($f = 0.002$)).

The analyses of TD-DFT results display that the absorption spectra of the *E*-isomers are shifted to shorter wavelengths than those of *Z*-isomers (see Fig. S3, ESI[†]). This is in agreement with the existing experimental results and theoretical study at the ω B97XD/def2-SVPP level proposed by Mravc *et al.*²⁵ Furthermore, the experimental $S_0 \rightarrow S_1$ transition energy of 1 and 7 isomers show red-shift energy absorption compared to TD- ω B97XD calculation by about 0.12 eV (for *E1* and *E7*) and 0.55 eV (*Z1* and *Z7*) (see Table 5).

For the *E* isomers ($i = 1\text{--}9$), the wavelength of the first absorption transition is very close to that of the *E*-isomers (10 to 18, respectively). The same observation is found for *Z* isomers (i from 1 to 18), indicating that the introduction of NO_2 or CN group at the R position has little effect on the absorption wavelength of *E* and *Z* isomers. Taking *E6* and *E15*



Table 5 Vertical transition energy ($\Delta E_{0 \rightarrow 1}$, eV) and wavelength ($\Delta \lambda_{0 \rightarrow 1}$, nm), oscillator strengths (f , dimensionless), charge transfer (q^{CT} , $|e|$), charge transfer distance (d^{CT} , Å), and dipole moment variation ($\Delta \mu$, D) associated to the $S_0 \rightarrow S_1$ transition as calculated at the ωB97XD/6-311+g(d) in *Ei* and *Zi* compounds

	$\Delta E_{0 \rightarrow 1}$	$\Delta \lambda_{0 \rightarrow 1}$	f	d^{CT}	q^{CT}	$\Delta \mu$
<i>E1</i>	3.798(3.67) ^a	326	0.316	5.690	0.755	20.640
<i>E2</i>	3.780	327	0.315	5.884	0.767	21.671
<i>E3</i>	4.002	309	0.002	2.245	0.753	8.114
<i>E4</i>	3.931	315	0.463	4.771	0.666	15.252
<i>E5</i>	3.945	314	0.697	4.366	0.612	12.832
<i>E6</i>	3.844	322	0.923	2.335	0.674	7.557
<i>E7</i>	3.971(3.85) ^a	312	0.314	3.549	0.670	11.126
<i>E8</i>	3.556	348	0.56	3.659	0.663	10.590
<i>E9</i>	3.537	350	0.441	2.002	0.566	5.440
<i>Z1</i>	3.60(3.05) ^a	343	0.673	5.092	0.710	17.368
<i>Z2</i>	3.477	356	0.727	5.477	0.676	17.771
<i>Z3</i>	3.878	319	0.662	5.239	0.669	16.830
<i>Z4</i>	3.693	335	0.752	5.130	0.691	17.020
<i>Z5</i>	3.655	339	0.879	5.600	0.688	18.496
<i>Z6</i>	3.601	344	0.960	4.205	0.665	13.435
<i>Z7</i>	3.751(3.20) ^a	330	0.696	5.250	0.695	17.516
<i>Z8</i>	3.384	366	0.706	5.096	0.660	16.146
<i>Z9</i>	3.364	368	0.638	4.519	0.562	12.204
<i>E10</i>	3.962	312	0.615	4.256	0.672	13.736
<i>E11</i>	3.883	319	0.609	4.562	0.690	15.111
<i>E12</i>	4.370	283	0.635	3.651	0.601	10.543
<i>E13</i>	4.044	306	0.754	3.666	0.611	10.755
<i>E14</i>	3.998	310	0.934	3.368	0.566	9.165
<i>E15</i>	3.879	319	1.013	2.666	0.599	7.676
<i>E16</i>	4.092	302	0.690	3.749	0.589	10.600
<i>E17</i>	3.580	346	0.604	1.803	0.542	4.694
<i>E18</i>	3.540	350	0.430	3.120	0.509	7.629
<i>Z10</i>	3.642	340	0.659	3.551	0.608	10.370
<i>Z11</i>	3.519	352	0.704	4.509	0.649	14.044
<i>Z12</i>	3.925	315	0.627	3.078	0.561	8.291
<i>Z13</i>	3.718	333	0.743	3.242	0.587	9.146
<i>Z14</i>	3.6716	337	0.867	3.374	0.578	9.365
<i>Z15</i>	3.617	342	0.958	0.390	0.558	1.046
<i>Z16</i>	3.7940	326	0.6899	3.449	0.574	9.507
<i>Z17</i>	3.409	363	0.680	2.480	0.552	6.575
<i>Z18</i>	3.383	366	0.6262	0.740	0.502	1.783

^a Experimental results from ref. 25.

as example, the $\lambda_{0 \rightarrow 1}$ is 322 and 315 nm, respectively, and for *Z6* and *Z15*, the $\lambda_{0 \rightarrow 1} = 343$ nm for both (see Fig. 4). On the other hand, the TD-DFT calculation on the title isomers reveals that the low-energy transitions $S_0 \rightarrow S_1$ are dominated by an electronic excitation from the HOMO to the LUMO, and the shape of these two MOs depicts a significant charge transfer (CT) from the hydrazine part and ring 1 to ring 2 for the compounds 1, *E2*, 3, 4, *Z5-Z10*, *E11*, 12, 13, *E14*, *Z15*, 16, *Z17*, and *Z18*, and the CT character from the hydrazine part to ring1 for the isomers *Z2*, *Z11*, and *Z14* (see Table S3 and Fig. S1, S2, ESI[†]) and intramolecular charge transfer (ICT) in the hydrazine part and ring1 for *E5*, *E6*, *E8*, *E9*, *E15*, *E17*, and *E18* isomers. For the isomers 1–9 (substituted with NO_2 at the *R* position), the HOMO \rightarrow LUMO+1 transition mainly results from the Ar group to ring1, with the exception of the isomers *E5*, *E6*, *E8*, *E9*, and *Z6*, which exhibit an ICT character in the ring1 and Ar groups. On the other hand, for the isomers with the CN unit at the *R* position, the HOMO \rightarrow LUMO+1 transition can also be assigned as $n, \pi \rightarrow \pi^*$ but from the Ar group to the ring2, with the exception for *Z18* and *E18*, which exhibit an ICT character (see Table S3 and Fig. S1, ESI[†]).

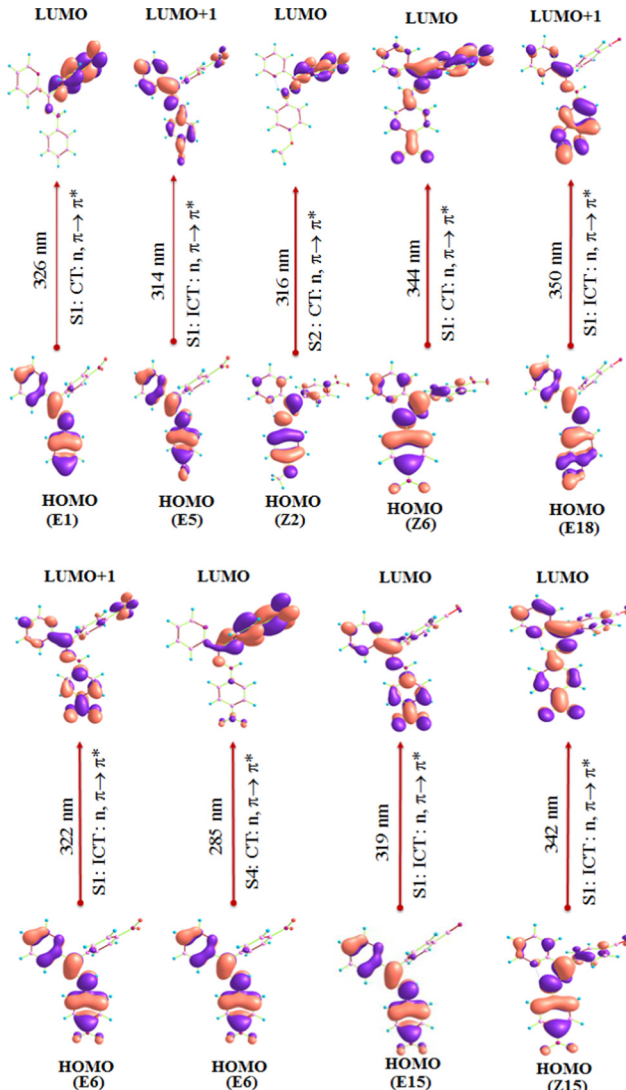


Fig. 4 Molecular orbitals for *S1*, *S2*, and *S4* absorption transitions.

In the case of *Zi* and *Ei* isomers ($i = 1$ to 9), it is clear that the transition HOMO \rightarrow LUMO results in a more significant dipole moment ($\Delta \mu$) compared to the transition HOMO \rightarrow LUMO+1. Conversely, for the remaining compounds (10 to 18) substituted with a CN group at the position *R*, the reverse pattern is observed (see Table S3, ESI[†]). Taking *Z2* and *Z11* as an example (see Fig. 5), for *Z2*, the order of $\Delta \mu$ values follows the order $\Delta \mu_{02}(\text{H} \rightarrow \text{L}: 20.19) > \Delta \mu_{01}(\text{H} \rightarrow \text{L+1}: 17.77)$, and the reverse order is found for *Z11* $\Delta \mu_{02}(\text{H} \rightarrow \text{L+1}: 21.72) > \Delta \mu_{01}(\text{H} \rightarrow \text{L}: 14.04)$. In general, for the same transition HOMO \rightarrow LUMO, LUMO+1, the $\Delta \mu$ values is larger in the 1–9 isomers than that in the corresponding 10–18 isomer, indicating that the presence of the NO_2 group can enhance the $\Delta \mu$ and q^{CT} values more than the CN group. For example, *Z2* (17.77 D) is due to a transferred excitation charge $q^{CT} = 0.676|e|$, and an associated CT distance ($d^{CT} = 5.477 \text{ \AA}$) from HOMO to LUMO+1 ($S_0 \rightarrow S_1$) is larger than that of the excitation $S_0 \rightarrow S_1$ (from HOMO to LUMO) of *Z11* ($q^{CT} = 0.649|e|$, $d^{CT} = 4.509 \text{ \AA}$ and $\Delta \mu_{0 \rightarrow 1} = 14.04 \text{ D}$). Generally, for the title photoswitch compounds, we note that the *Z*-isomer



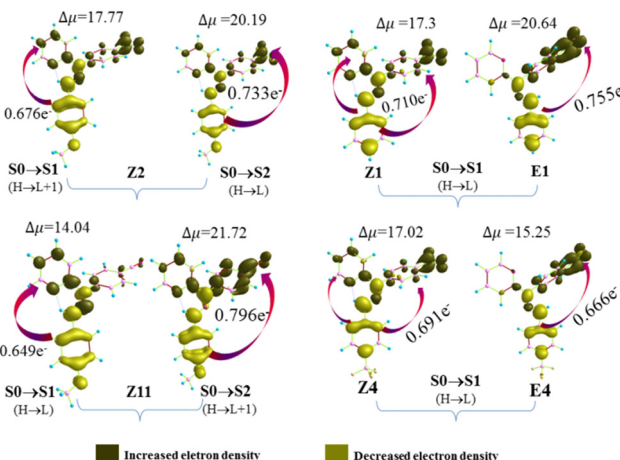


Fig. 5 Electron density difference maps of Z_1 , E_1 , Z_2 , Z_4 , E_4 , and Z_{11} compounds from the ground state to the crucial excited state $S_0 \rightarrow S_1$ and $S_0 \rightarrow S_2$.

undergoes a strong CT excitation with a large CT distance (d^{CT}) and dipole moment variation ($\Delta\mu$) compared to the *E*-isomers counterpart (compounds 1, 2, and 15 are exceptions to this, see Table S3, ESI[†]). For instance, the $\Delta\mu_{0 \rightarrow 1}$, d^{CT} and q^{CT} of Z_4 are calculated to be 17.02 D, 5.13 Å, and $0.691|e|$ larger than the corresponding values of E_4 (Fig. 5). Conversely, the $\Delta\mu$, d^{CT} , and q^{CT} of Z_1 and Z_2 show small values with respect to that of E_1 and E_2 (Fig. 5 and Table S3, ESI[†]). It appears that the shape of the *Z*-isomer significantly increases the $\Delta\mu$, d^{CT} , and q^{CT} values, which can be attributed to the electron delocalization effects in the ring N1–N2–C3–C4–N6···H (RAHB system).

Based on the quantum calculation, it can be observed that the strength of the hydrogen bond does not exert a significant effect on the optical properties of photoswitches (Table 5). Instead, the optical properties are influenced by conjugation, which is determined by the structure of the quasi-cycle (open or closed). It is crucial to emphasize that the opening or closing of the RAHB can significantly impact various molecular properties, including stability, acidity, basicity, reactivity, and optical properties.

Nonlinear optical properties

Dipole moment (μ , eV), isotropic polarizability (α), polarizability density (ρ a.u. Å⁻³), nonlinear optical responses (NLO), *e.g.*, first hyperpolarizability (β_0 , a.u), second harmonic generation (β_{SHG} , a.u), electrooptic Pockels effect (β_{EOP} , a.u), Hyper-Rayleigh scattering (β_{HRS} , a.u), and depolarization ratio DR (static as well as dynamic) for all isomers are provided in Tables 6 and 7 and Tables S3, S4 and S5 (see ESI[†]).

The static and dynamic results for average linear polarizability ($\langle\alpha\rangle$) and dipole moment (μ) are presented in Tables 6 and 7, respectively. Molecular polarizability is the ability of its electronic system to be distorted by an external field; according to our results in Table 6, the $\langle\alpha\rangle$ value of the *Z*-isomer is slightly larger than the *E*-isomer counterpart. On the other hand, the most polarizable isomers are 8 and 17. These results show that

Table 6 Static and dynamic isotropic average polarizability (α) and isotropic average polarizability volume (ρ) of E_i and Z_i ($i = 1$ to 18) compounds

	$\lambda = \infty$		$\lambda = 695$		$\lambda = 1064$		$\lambda = 1340$	
	α	ρ	α	ρ	α	ρ	α	ρ
E_1	265	39	283	41	272	40	269	39
E_2	284	42	302	44	291	43	289	42
E_3	259	38	273	40	264	39	262	38
E_4	280	41	297	44	287	42	284	42
E_5	289	42	310	45	297	44	294	43
E_6	291	43	313	46	300	44	296	43
E_7	259	38	276	40	266	39	263	39
E_8	313	46	336	49	322	47	319	47
E_9	306	45	329	48	315	46	311	46
Z_1	276	40	299	44	285	42	281	41
Z_2	301	44	328	48	311	46	307	45
Z_3	270	40	288	42	277	41	274	40
Z_4	290	42	312	46	298	44	295	43
Z_5	300	44	325	48	309	45	306	45
Z_6	301	44	329	48	311	46	307	45
Z_7	268	39	289	42	276	41	273	40
Z_8	325	48	355	52	336	49	332	49
Z_9	317	47	348	51	329	48	325	48
E_{10}	265	39	282	41	272	40	270	40
E_{11}	285	42	303	45	292	43	290	42
E_{12}	259	38	270	40	264	39	262	38
E_{13}	280	41	297	44	286	42	284	42
E_{14}	290	43	310	45	298	44	295	43
E_{15}	292	43	313	46	300	44	297	44
E_{16}	260	38	276	40	266	39	264	39
E_{17}	313	46	337	49	322	47	319	47
E_{18}	306	45	329	48	315	46	312	46
Z_{10}	275	40	297	44	284	42	281	41
Z_{11}	299	44	325	48	309	45	306	45
Z_{12}	269	39	286	42	276	40	273	40
Z_{13}	288	42	310	45	297	44	294	43
Z_{14}	300	44	325	48	310	45	306	45
Z_{15}	301	44	328	48	312	46	308	45
Z_{16}	268	39	288	42	276	40	273	40
Z_{17}	324	48	353	52	335	49	331	49
Z_{18}	317	47	346	51	328	48	324	48

Table 7 Calculated dipole moment (μ , Debye), static hyperpolarizability (β_0 , $\beta_{HRS}^{i=\infty}$ a.u), and depolarization ratio (DR) calculated at the ω B97XD/6-311+g(d) level for E_i and Z_i ($i = 1$ to 18) compounds

	μ	β_0	$\beta_{HRS}^{i=\infty}$	DR $^{i=\infty}$		μ	β_0	$\beta_{HRS}^{i=\infty}$	DR $^{i=\infty}$
E_1	5.098	1608	756	3.562	Z_1	7.176	3906	1618	4.991
E_2	5.340	2246	963	4.48	Z_2	8.476	6498	2536	6.275
E_3	4.980	1024	474	3.672	Z_3	7.736	2965	1217	5.143
E_4	5.035	1052	585	2.693	Z_4	8.572	2980	1264	4.623
E_5	6.282	312	546	1.584	Z_5	9.924	2202	1055	3.428
E_6	6.604	1928	1101	2.607	Z_6	1.019	1530	1152	2.756
E_7	7.080	995	553	2.695	Z_7	5.343	2898	1261	4.294
E_8	6.047	1446	730	3.114	Z_8	7.510	3970	1674	4.711
E_9	3.500	639	689	1.735	Z_9	8.981	2570	1230	3.438
E_{10}	4.905	1510	702	3.648	Z_{10}	6.936	2632	1067	5.374
E_{11}	5.261	2156	912	4.660	Z_{11}	8.188	5017	1933	6.664
E_{12}	4.870	845	387	3.765	Z_{12}	7.649	1901	760	5.655
E_{13}	4.992	987	529	2.829	Z_{13}	8.516	1810	757	4.844
E_{14}	6.293	683	548	1.959	Z_{14}	9.853	1107	615	2.696
E_{15}	6.626	2293	1164	3.085	Z_{15}	1.020	1488	996	2.219
E_{16}	6.895	936	497	2.871	Z_{16}	5.114	1732	757	4.246
E_{17}	5.888	1339	666	3.196	Z_{17}	7.258	2390	1000	4.825
E_{18}	3.398	1126	757	2.211	Z_{18}	8.867	1160	646	2.689

the presence of the Ar₈ group can enhance the polarizability value. The calculation shows that the polarizability density

values (ρ) are similar and not sensitive to the type of Ar and R groups. Furthermore, we observed that the effect of the incident wavelength value ($\lambda = 1340, 1064$, and 695 nm) on $\langle\alpha\rangle$ and $\langle\rho\rangle$ is negligible.

As is well known, the hyperpolarizability is sensitive to the several parameters such as the nature of the substituent (donor/acceptor), geometry of compounds, transition dipole moment, energy gap, electronic transition, and incident wavelength (photon energy). From Table S3, ESI[†] and Fig. 6, one sees that the $\beta_{\text{HRS}}^{\lambda=695}$ and β_0 values of *E*-isomers substituted by either CN group or by NO_2 are very close, indicating that the replacement of NO_2 by CN group (at R position) has no effect on the static hyperpolarizability. Taking *E*8 and *E*17 as examples, $\beta_{\text{HRS}}^{\lambda=695}(\text{E}8) = 1.09 \beta_{\text{HRS}}^{\infty}(\text{E}17)$. But in the case of *Z*-isomers, the introduction of the NO_2 acceptor substituent at the R position can increase the static hyperpolarizability ($\beta_{\text{HRS}}^{\infty}$ and β_0) about twice more than that of the CN group, with the exception of *Z*6 and *Z*15 compounds, for which their values are close ($\beta_0(\text{Z}6) = 1.028\beta_0(\text{Z}15)$), an effect which can be attributed to the small dipole moment ($\mu = 1.01$ D). Furthermore, we can observe that the introduction of Ar_2 groups can increase the $\beta_{\text{HRS}}^{\infty}$ and β_0 compared with the Ar_3 and Ar_5 groups (Fig. 6 and Table 7). For example, the β_0 value of *E*2, *Z*2, *E*11, and *Z*11 is about 7, 4, 3, and 4 times larger than that of *E*5, *Z*5, *E*14, and *Z*14, respectively. The $\beta_{\text{HRS}}^{\infty}$ of *Z*2 (2536 a.u.) and *Z*11 (1933) are about 7 and 5 times greater than the values of *E*12, respectively (Fig. 6).

Also, in this work, we studied the correlation between the energy gap (hardness) of *Zi* and *Ei* isomers and their hyperpolarizability in the static regime. The results show that the $\beta_0[\beta_{\text{HRS}}^{\infty}]$ values increase with the decrease in the isomer energy gap. Taking *Z*2 as an example, the energy gap of *Z*2 is the smallest (6.304 eV) and its hyperpolarizability value is the largest ($\beta_0 = 6498$ a.u.), which is in good agreement with the literature.^{74–77}

The magnitude of the hyperpolarizabilities of hydrazone photoswitches can be qualitatively rationalized using the two-state approximation, assuming that the S1 electronic excited state is the sole contributor to the sum-over-state expansion of

the second-order nonlinear optical (NLO) response.^{78,79}

$$\beta = \frac{3f_{0 \rightarrow 1} \times \Delta\mu_{0 \rightarrow 1}}{2 \Delta E_{0 \rightarrow 1}^3}$$

According to this formula, β is directly linked to the transition dipole moment $\Delta\mu_{0 \rightarrow 1}$ and oscillator strength $f_{0 \rightarrow 1}$ and inversely linked to the third power of transition energy $\Delta E_{0 \rightarrow 1}$.

Based on our findings from Table 5 and Table S3 (ESI[†]), it is evident that the *Z* isomer exhibits a lower excited energy ($\Delta E_{0 \rightarrow 1}$) and higher oscillator strength ($f_{0 \rightarrow 1}$) compared to its *E*-isomer counterpart. Our results clearly show that a decrease in the $\text{S}0 \rightarrow \text{S}1$ transition energy and an increase in the value of $f_{0 \rightarrow 1}$ are directly associated with an increase in the hyperpolarizabilities of hydrazone photoswitches. Taking *E*1 and *Z*1 as example, *E*1 has a transition energy value of 3.798 eV, while *Z*1 has a lower value of 3.606 eV, and the $f_{0 \rightarrow 1}$ value of *Z*1 is higher than that of *E*1. The DFT calculation shows that *Z*1 exhibits a larger hyperpolarizability value compared to the *E*1 isomer. Similarly, we observed the same trend for the other isomers. Each isomer exhibits a lower transition energy ($\Delta E_{0 \rightarrow 1}$) and huge $f_{0 \rightarrow 1}$ value, generally displaying larger hyperpolarizability compared to its counterpart.

On the other hand, the larger hyperpolarizability values in the *Z*-isomers, compared to those in the *E*-isomers, can be due to the delocalization of electrons in the anti-aromatic QCC (N1–N2–C3–C4–N6···H) in the *Z*-isomers, which does not exist in the *E*-isomers (Fig. 1, Table 2 and Table S1, ESI[†]). It means that destabilizing the anti-aromatic behavior of quasi-cycle closed in the *Z*-isomers can reduce and grow the aromatic character in ring 2 and 1, respectively, and this leads to enhanced hyperpolarizability values.

From our calculation, we observe that when the compound is in a *Z* form, the BLA decreases, which indicates a better electron delocalization and, consequently, the hyperpolarization increases. Fig. 7 presents a nice linear relationship between BLA_{1-2} and static hyperpolarizability $\beta_{\text{HRS}}^{\infty} [\beta_0]$ of *Z*-isomers. It is important to note that for the title isomers, the variations of $\beta_{\text{HRS}}^{\infty}$ values are similar to those of β_0 values.

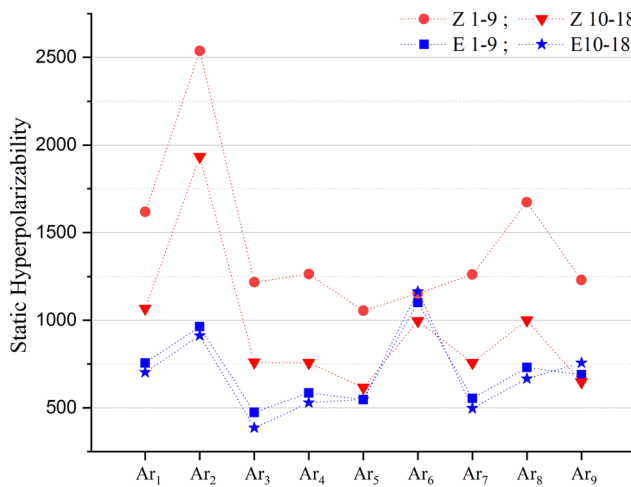


Fig. 6 Variation of HRS hyperpolarizability in static regime of *Z* and *E* isomers.

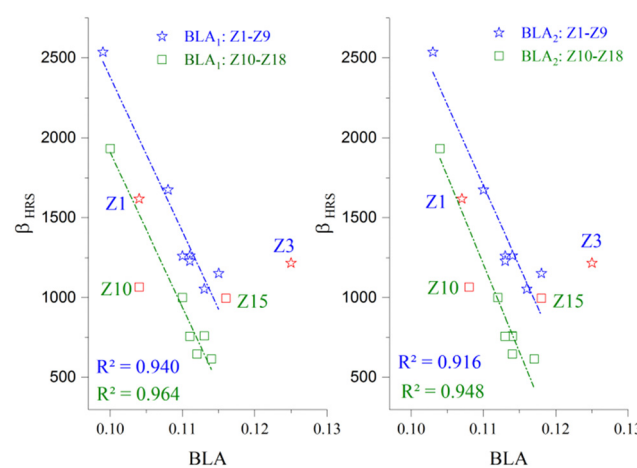


Fig. 7 Correlation between BLA and static hyperpolarizability; the red points have been omitted from the correlation line.



Generally, the TD-DFT results indicated that the *Z*-isomers have low excitation energies of the first excited state and large transition dipole moments ($\Delta\mu$), which are the necessary conditions to obtain high NLO response.

Mravec research group showed that increasing the EW character of the substituents on the Ar-ring leads to a little increase in the efficiency of the $Z \rightarrow E$ photoisomerization, whereas a large increase in the quantum yield can be observed in the case of the back $E \rightarrow Z$ photoisomerization (in the order $3 > 5 > 4 > 7 > 1 > 6 > 2$; see Fig. 8).²⁵ In general, our quantum calculation show inverse trend between the photoisomerization quantum yields (Φ) and hyperpolarizability. Note, for instance, compound 2 (see Table 7 and Fig. 6), which has the largest hyperpolarizability and the smallest photoisomerization QY (the EW substituents on the $-C_6H_4$ is OCH_3 ; $Ar_2 = -C_6H_4-\rho-OCH_3$). Furthermore, the trend photoisomerization QY is the same as that for the BLA values (see Table 1). On the other hand, we can attribute the small and large photoisomerization QY values ($\Phi_{Z \rightarrow E} < \Phi_{E \rightarrow Z}$) to the hyperpolarizability of the first and second isomer of the mechanism. In other words, the $Z \rightarrow E$ photoisomerization mechanism²⁵ begins with the isomer having the largest hyperpolarizability (first isomer *Z*) and finishes with the *E*-isomer (second isomer) that has a small hyperpolarizability; this mechanism displays a weak $\Phi_{Z \rightarrow E}$ value. In the same context, $E \rightarrow Z$ photoisomerization starts with the *E*-isomers (first isomer) having the smaller hyperpolarizability than the second isomer *Z* and present a larger $\Phi_{E \rightarrow Z}$ value than $\Phi_{Z \rightarrow E}$ (see Tables 7, 8 and Fig. 8). Taking compound 3 as an example, the photoisomerization quantum yields of $\Phi_{E3 \rightarrow Z3}$ are larger than that of $\Phi_{Z3 \rightarrow E3}$ ($\Phi = 12.3$ and 0.8, respectively),²⁵ and the hyperpolarizability value of *Z*3 is larger than that of *E*3 ($\beta[Z3] \approx 3\beta[E3]$) (see Table 8).

From our study, we can conclude that there is a proportional relationship between photoisomerization quantum yield and hyperpolarizability of the second isomer, and there is an

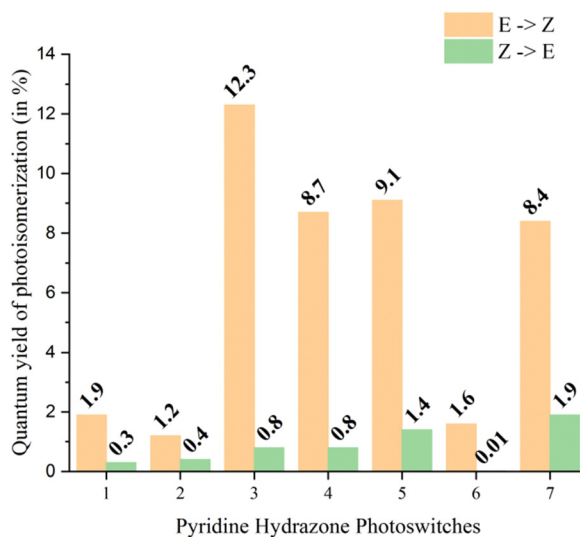


Fig. 8 Evolution of photoisomerization quantum yields (Φ) with the increasing EW character of the hydrazine ring (the values from the ref. 25).

Table 8 The static and dynamic hyperpolarizability β_Z^2/β_{Ei}^2 ratio (where $\eta^2 = \beta_Z^2/\beta_{Ei}^2$; η_{HRS}^{∞} , η_0 and η_{SHG}^{∞}) to the *Z*- and *E*-isomers

<i>Zi/Ei</i>	η_{HRS}^{∞}	η_{HRS}^{695}	η_{HRS}^{1064}	η_{HRS}^{1307}	η_0	η_{SHG}^{695}	η_{SHG}^{1064}	η_{SHG}^{1307}
1	2.140	14.097	2.385	2.267	2.429	13.464	2.541	2.465
2	2.633	6.485	3.131	2.883	2.893	5.854	3.312	5.713
3	2.567	5.578	2.980	2.780	2.895	5.597	3.224	3.051
4	2.160	6.191	2.4656	2.328	2.832	6.107	2.809	2.766
5	1.932	10.947	2.7012	2.357	7.057	11.286	5.252	5.943
6	1.046	6.083	1.034	1.037	0.793	4.287	0.733	0.754
7	2.280	4.939	2.555	2.434	2.912	4.863	2.854	2.837
8	2.293	0.221	2.792	2.556	2.745	0.184	3.059	2.893
9	1.785	0.212	2.191	2.012	4.021	0.076	4.732	4.496
10	1.519	7.919	1.739	1.636	1.743	7.936	1.915	1.829
11	2.119	11.437	2.442	2.280	2.326	11.102	2.593	2.450
12	1.963	4.078	2.237	2.108	2.249	4.275	2.492	2.366
13	1.431	4.866	1.705	1.577	1.833	4.982	2.001	1.908
14	1.122	8.439	1.667	1.391	1.620	9.172	2.681	2.304
15	0.855	2.092	0.7881	0.817	0.648	0.753	0.550	0.592
16	1.523	3.438	1.727	1.634	1.850	3.553	1.968	1.906
17	1.501	0.169	1.767	1.631	1.784	0.151	2.001	1.880
18	0.853	0.078	0.941	0.901	1.030	0.059	1.276	1.192

inversely proportional relationship between the Φ and β of the first isomer. These relationships will be the object of further investigations.

According to the TD-DFT results ($\lambda_{Max} \equiv \lambda_{0 \rightarrow 1}$), we calculated the hyperpolarizability (β_{HRS}^2 , β_{SHG}^2 , and β_{EOPE}^2) of the studied isomers at a near resonant wavelength of 695 nm ($\approx 2 \times \lambda_{Max}$) and a nonresonant wavelength of 1064 nm and 1340 nm. Our results from the dynamic regime present an excellent linear relationship between Hyper-Rayleigh scattering (β_{HRS}^2) and second harmonic generation (β_{SHG}^2) (see Fig. 9).

As can be seen in Fig. 10, the hyperpolarizability value increases with decreasing wavelength of the incident light, i.e., $\beta(695) > \beta(1064) > \beta(1340) > \beta(\infty)$. Obviously, the β_{SHG}^2 and β_{HRS}^2 values dramatically increase at the 695 nm wavelength more than at $\lambda = 1340$ nm and 1064 nm, which can be attributed to the larger resonance or dispersion at 290–366 nm according to the TD-DFT results (Table S3, ESI†). As examples, *Z*1 exhibits the largest response at $\lambda = 695$ nm

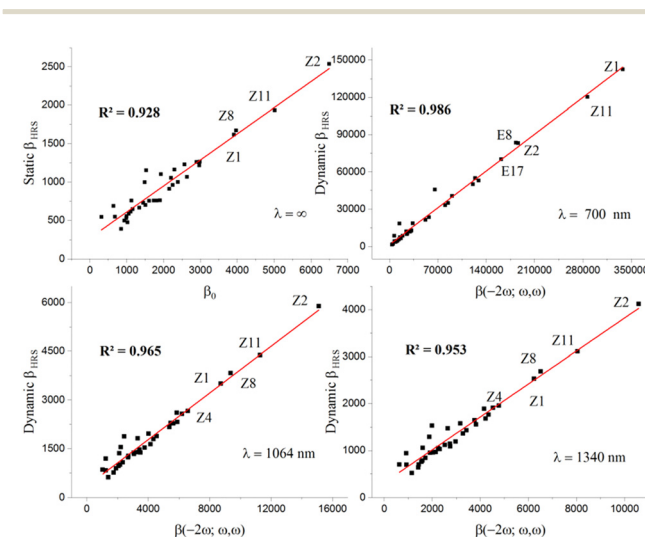


Fig. 9 Correlation between $\beta_{HRS}^2 \leftrightarrow \beta_0$ and $\beta_{HRS}^2 \leftrightarrow \beta_{SHG}^2$.

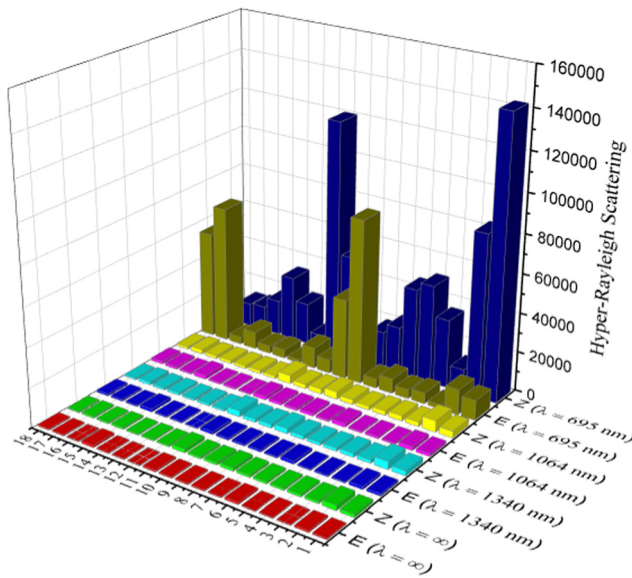


Fig. 10 Calculated first hyperpolarizabilities of *Z* and *E* isomers, in the zero frequency limit and frequency-dependent fields.

$\beta_{\text{HRS}}^{695}[\beta_{\text{SHG}}^{695}] = 142\,500[337\,600]$ a.u.), while this isomer possesses small values at $\lambda = \infty$, 1340, and 1064 nm. By way of explanation, the hyperpolarizability $\beta_{\text{HRS}}^2[\beta_{\text{SHG}}^2]$ of *Z1* at 695 nm is approximately 39 and 55 times higher than at 1340 and 1064 nm, respectively. On the other hand, the magnitude of $\beta(-\omega; \omega, 0)$ is slightly enhanced with increasing frequency of the incident light compared with β_{HRS}^2 and β_{SHG}^2 (Table S4, ESI†). Taking *Z2* and *E5* as examples, the $\beta_{\text{EOPE}}^{695}$ value of *Z2* (12100 a.u.) is evaluated to be the largest, and *E5* possess a small value of $\beta_{\text{EOPE}}^{695}$ (771 a.u.), which is almost two times larger than that of the β_{EOPE}^2 at 1340 and 1064 nm.

In most cases in static and dynamic regime ($\lambda = \infty$, 1064, and 1307 nm), the hyperpolarizability β_0 , β_{SHG}^2 , β_{HRS}^2 of *Z*-isomers are in the range of 2–7 times as large as those of the corresponding *E*-isomer. For example, the β_0 value of *Z5* is 2200 a.u., which is 7 times larger than that of the corresponding *E5*. With the exception of compounds 6, 15, and 18, where the values of *Z* are smaller than that of *E*, for instance, $\beta_{\text{SHG}}^2(\text{Z15})/2\beta_{\text{SHG}}^2(\text{E15})$ (see Table 8). On the other hand, the $\beta_{\text{SHG}}^{695}[\beta_{\text{HRS}}^{695}]$ of *Z*-isomers is 2–14 times larger than that of the corresponding *E*-isomers. With the exception of compounds 8, 9, 17, and 18, where *E8*, *E9*, *E17*, and *E18* have the largest $\beta_{\text{SHG}}^{695}[\beta_{\text{HRS}}^{695}]$ value, which is about 5, 13, 7, and 17 [5, 5, 6, and 13] times as large as those of the *Z*-isomers *Z8*, *Z9*, *Z17*, and *Z18*, respectively (Table 8).

In addition, dynamic perturbations were introduced to explore the effect of frequency dispersion. To provide a comparison, we utilized two fundamental optical wavelengths $\lambda = 1340$ and 1064 nm (used in NLO measurements) along with 695 nm (derived from TD-DFT results). This allowed us to assess the contribution of dispersion correction to the NLO response in these isomers. To quantify this correction, we used the frequency dispersion factor between static and dynamic at a definite wavelength, which is depicted by the ratio $\beta_{\text{HRS}}^2/\beta_{\text{HRS}}^{695}$

and is listed in Table S6 (ESI†). We can observe that the dispersion of optical nonlinearity at $\lambda = 695$ nm of *E8*, *E17*, *Z1*, *E18*, *Z11*, *E9*, *Z14*, *Z10*, *Z5*, *Z6*, and *Z2*, respectively, have maximum frequency dispersion factor (from 115 to 32), which can be attributed to the TD-DFT results, where $\lambda_{\text{Max}} = \sim 695$ nm. In contrast to the isomers *E3* and *E12* ($\lambda_{\text{Max}} = 309$ and 283 nm, respectively), the smallest dispersion factor (about 4.36) and the other isomers show a moderate values (from 6 to 29) at $\lambda = 695$ nm. As can be seen, the frequency dispersion factor at incident laser ($\lambda = 1340$ and 1064 nm) of the title compounds is in the range of 1–5.

Our findings indicate that the frequency dispersion factor is greater at higher frequencies compared to lower frequencies; the weak frequency of incident light should be chosen to count the 2nd NLO coefficients in the experiment.⁸⁰ Regarding possible applications, in terms of writing and reading stored information on photochromic materials, the nonresonant character of NLO enables reading outside the absorption band; in this case, erasure during reading can be avoided.¹⁹ Clearly, the larger hyperpolarizability does emerge when the incident wavelength of dispersion is equal or closer to twice the wavelength in the first transition ($\lambda_{0 \rightarrow 1}$).

To further explore the origin of the first hyperpolarizability of the title compounds (*E* and *Z* isomers), the polarization scan of HRS intensity $I_{\Psi}^{2\omega}$ has also been calculated, and the relationship between the $I_{\Psi}^{2\omega}$ and polarization angle Ψ is plotted (see Fig. S5, ESI† and plotted for the compounds 1 and 5 in Fig. 11); the $\beta_{j=1}$ and $\beta_{j=3}$ are listed in Table S5 (ESI†).

From Fig. 12, we can conclude that the DR values are sensitive to the nature of the Ar and R substituents, the geometry of isomers (*Z* and *E* shapes), as well as the wavelength of incident light. We observed that at $\lambda = \infty$, 1064, and 1307 nm, the DR value decreases in the following order: DR ($\lambda = 1064$) > DR ($\lambda = 1340$) > DR ($\lambda = \infty$) also; from this figure,

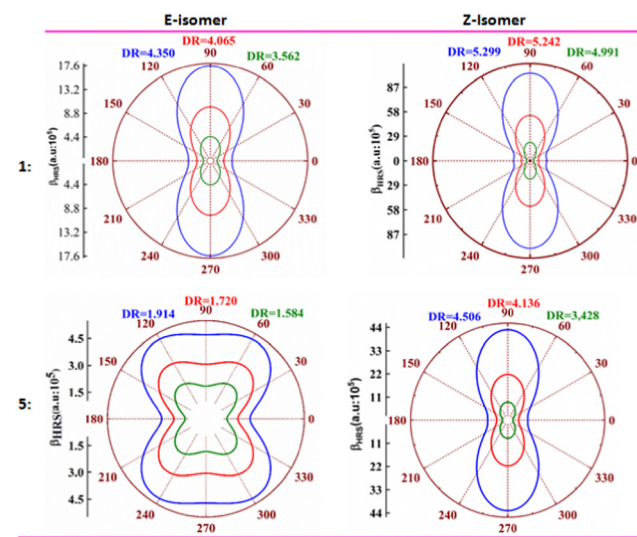


Fig. 11 Relationship between $I_{\Psi}^{2\omega}$ and polarization angle Ψ of *Z* and *E* isomers (green static, red $\lambda = 1340$ nm, blue $\lambda = 1064$ nm).



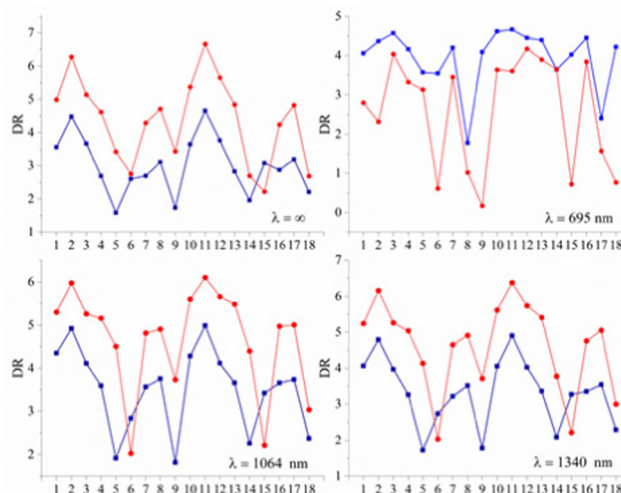


Fig. 12 Evolution of the depolarization ratio (DR) in static and dynamic regime (red: Z-isomer, blue: E-isomer).

it seems that the Z-isomer exhibits larger DR than the corresponding E-isomer. In contrast, at 695 nm, the depolarization ratio of E-isomer is larger than that of the Z-isomer counterpart, which can be attributed to its resonance or dispersion at λ_{Max} .

On the other hand, at $\lambda = \infty$, 1064, and 1307 nm, it can be found that E4, E13, E6, Z6, E15, Z15, E7, E16, E8, E17, E9, E18, and Z18 molecules are considered as octupolar molecules with large octupolar contributions ($\beta_{J=3} > \beta_{J=1}$), while E1, E10, Z10, E2, Z2, E11, Z11, E3, Z3, E12, Z12, Z4, Z13, Z5, Z7, Z16, Z8, Z17, Z9 molecules are considered as dipolar molecules and dipolar contributions, with $\beta_{J=1}$ larger than the $\beta_{J=3}$ (see Table S5 and Fig. S5, ESI†). For Z1 and E5, as illustrated in Fig. 11, the DR amounts to 4.991 and 1.584, respectively, a value close to 5 and 1.5; these values characterize ideal dipolar and typical octupolar systems, respectively.

The quantum chemical calculation shows that the Z-isomers exhibit the largest response, whereas the corresponding E-isomers exhibit smaller values at static and dynamic regimes. It is worth noting that the larger NLO responses are strongly related to the hydrogen bond, the electron-withdrawing character of the substituents on the Ar hydrazine moiety, and on the ring 2, the photoisomerization quantum yields $\Phi_{E \rightarrow Z}$. Among the 18 E/Z isomers theoretically studied, Z2 is the most promising for future applications in the NLO field.

Conclusions

Systematic DFT and TD-DFT calculations have been carried out on extended series of substitutional derivatives of pyridine photoswitches. The structural, reactivity parameters, linear, and nonlinear optical properties of all compounds differing by a CN and NO₂ substitution on the ketone fragment at the position R and Ar ring in the hydrazine fragment have been analyzed in detail.

The quantum calculation indicates that the Z-isomers are proposed to be a promising candidate for the 2nd order

nonlinear optical applications due to its lower excited energy, smaller BLA values, weaker energy gap, larger dipole moment variations in the first excited state, smaller electron localization in the anti-aromatic ring (QCC), and higher photoisomerization quantum yields $\Phi_{E \rightarrow Z}$ than that of the corresponding E-isomers. To the best of our knowledge, this work evidences that the delocalization strength enhanced by the resonance-assisted hydrogen bond can improve the second order NLO responses of the hydrazone photoswitches, especially due to the delocalized electrons in the anti-aromatic ring (QCC) in Z-isomers.

Regarding the NLO properties, DFT calculation indicates that the CN and NO₂ groups have the same effect on the static hyperpolarizability of E-isomers. For Z-isomers, the introduction of NO₂ at R position increases the $\beta_{\text{HRS}}^{\infty}$ and β_0 to about twice more than that of the CN group. Furthermore, their introduction into the Ar₂ group increases the hyperpolarizability ($\beta_{\text{HRS}}^{\infty}$ and β_0) compared with Ar₃ and Ar₅ groups.

Regarding the nonlinear optical properties of isomers, we found that the frequency-dependent hyperpolarizability ($\lambda = 695$ nm) of the title isomers are larger than the static regime, revealing an eminent hyperpolarization due to the delocalized electrons in the isomers. By increasing the incident wavelengths from $\lambda = 695$ nm to $\lambda = 1064$ and 1307 nm, the dispersion of optical nonlinearity of isomers shows a smaller value than that at $\lambda = 695$ nm. Our results indicate that the resonance effect of hyperpolarizability is amplified with the decrease in the incident wavelength ($\lambda = 695$ nm). A good correlation is obtained between $\beta_{\text{HRS}}^{\infty} \leftrightarrow \beta_0$ and $\beta_{\text{HRS}}^{\lambda} \leftrightarrow \beta_{\text{SHG}}^{\lambda}$ as well as between BLA and static hyperpolarizability.

Author contributions

All the authors discussed the results. Conceptualization and methodology: D. H. and H. C.; investigation: D. H., N. K., M. Z., D. Y., S. L., C. M. and H. C.; writing – original draft preparation: D. H. and H. C.; writing – review & editing: D. H., N. K., M. Z., D. Y., S. L.; C. M. and H. C.; data curation: D. H., N. K., M. Z., D. Y., S. L., C. M. and H. C. All authors have read and agreed to the published version of the manuscript.

Conflicts of interest

There are no conflicts to declare.

Acknowledgements

The authors gratefully acknowledge the GENCI/CINES for HPC resources/computer time (Project cpt2130), and the PSMN of the ENS-Lyon for computing resources.

Notes and references

- 1 K. Matsuda and M. Irie, *J. Am. Chem. Soc.*, 2000, **122**, 7195–7201.



2 C. G. Liu, Z.-M. Su, X.-H. Guan and S. Muhammad, *Mol. Phys.*, 2011, **115**, 23946–23954.

3 M. N. Chaur, D. Collado and J. M. Lehn, *Chem. – Eur. J.*, 2011, **17**, 248–258.

4 M. Schulze, M. Utecht, A. Hebert, K. Ru, P. Saalfrank and P. Tegeder, *J. Phys. Chem. Lett.*, 2015, **6**, 505–509.

5 L. Greb and J. Lehn, *J. Am. Chem. Soc. Irradiat.*, 2014, **136**, 13114–13117.

6 M. Zaidi, D. Hannachi, D. Samsar and H. Chermette, *Inorg. Chem.*, 2021, **60**, 6616–6632.

7 D. Kamli, D. Hannachi and H. Chermette, *New J. Chem.*, 2023, **47**, 1234–1246.

8 M. S. Kodikara, R. Stranger and M. G. Humphrey, *Coord. Chem. Rev.*, 2018, **375**, 389–409.

9 Y. Y. Liang, B. Li, X. Xu, F. Long Gu and C. Zhu, *J. Comput. Chem.*, 2019, **40**, 971–979.

10 N. Baggi, E. Garoni, A. Colombo, C. Dragonetti, S. Righetto, D. Roberto, J. Boixel, V. Guerchais and S. Fantacci, *Polyhedron*, 2018, **140**, 74–77.

11 C. Andraud, F. Cyril, B. Olivier, H. Chermette and P. L. Baldeck, *Adv. Polym. Sci.*, 2008, **214**, 149–203.

12 M. Schulze, M. Utecht, T. Moldt, D. Przyrembel, C. Gahl, M. Weinelt and P. Tegeder, *Phys. Chem. Chem. Phys.*, 2015, **17**, 18079–18086.

13 A. Goulet-hanssens and C. J. Barrett, *J. Polym. Sci., Part A: Polym. Chem.*, 2013, **51**, 3058–3070.

14 D. J. Van Dijken, P. Kovar, S. P. Ihrig and S. Hecht, *J. Am. Chem. Soc.*, 2015, **137**, 14982–14991.

15 K. J. Chen, A. D. Laurent and D. Jacquemin, *J. Phys. Chem. C*, 2014, **118**, 4334–4345.

16 P. Zhao, D. Wang, H. Gao, J. Zhang, Y. Xing, Z. Yang, H. Cao and W. He, *Dye. Pigment.*, 2018, **162**, 451–458.

17 A. J. Garza, O. I. Osman, N. A. Wazzan, S. B. Khan, G. E. Scuseria and A. M. Asiri, *Comput. Theor. Chem.*, 2013, **1022**, 82–85.

18 T. Woller, P. Geerlings, F. De Proft, B. Champagne and M. Alonso, *J. Phys. Chem. C*, 2019, **123**, 7318–7335.

19 J. A. Delaire, E. Ishow and K. Nakatani, *Photoreact. Org. Thin Film.*, 2002, 305–329.

20 L. Yan, T. Zhang and Z. Su, *J. Phys. Chem. A*, 2013, **117**, 10783–10789.

21 S. Ishihara, J. P. Hill, A. Shundo, G. J. Richards, J. Labuta, K. Ohkubo, S. Fukuzumi, A. Sato, M. R. J. Elsegood, S. J. Teat and K. Ariga, *J. Am. Chem. Soc.*, 2011, **133**, 16119–16126.

22 B. He and O. S. Wenger, *J. Am. Chem. Soc.*, 2011, **133**, 17027–17036.

23 Y. Zhang, H. Wang, J. Ye, X. Li and Y. Qiu, *Organomet. Chem.*, 2019, **888**, 29–36.

24 M. Samoc, N. Gauthier, M. P. Cifuentes, F. Paul, C. Lapinte and M. G. Humphrey, *Angew. Chemie*, 2006, **118**, 7536–7539.

25 B. Mravec, Š. Budzák, M. Medved, L. F. Paštka, C. Slavov, T. Saßmannshausen, J. Wachtveitl, J. Kožíšek, L. Hegedüsová, J. Filo and M. Cigáň, *J. Org. Chem.*, 2021, **86**, 11633–11646.

26 B. Mravec, J. Filo, K. Csicsai, V. Garaj, M. Kemka, A. Marini, M. Mantero, A. Bianco and M. Cigáň, *Phys. Chem. Chem. Phys.*, 2019, **21**, 24749–24757.

27 B. Mravec, A. Marini, M. Tommasini, J. Filo, M. Cigáň, M. Mantero, S. Tosi, M. Canepa and A. Bianco, *Chem. Phys. Chem.*, 2021, **22**, 533–541.

28 M. N. Chaur, D. Collado and J. M. Lehn, *Chem. – Eur. J.*, 2011, **17**, 248–258.

29 J. Da Chai and M. Head-Gordon, *Phys. Chem. Chem. Phys.*, 2008, **10**, 6615–6620.

30 J. Da Chai and M. Head-Gordon, *J. Chem. Phys.*, 2008, **128**, 084106–084114.

31 G. A. Petersson and A.-L. Mohammad, *J. Chem. Phys.*, 1991, **9**, 6081–6090.

32 G. A. Petersson, A. Bennett, T. G. Tensfeldt, M. A. Al-Laham, W. A. Shirley and J. Mantzaris, *J. Chem. Phys.*, 1988, **89**, 2193–2218.

33 S. Grimme, *J. Comput. Chem.*, 2006, **27**, 1787–1799.

34 M. J. Frisch, G. W. Trucks, H. B. Schlegel, G. E. Scuseria, M. A. Robb, J. R. Cheeseman, G. Scalmani, V. Barone, B. Mennucci, G. A. Petersson, H. Nakatsuji, M. Caricato, X. Li, H. P. Hratchian, A. F. Izmaylov, J. Bloino, G. Zheng, J. L. Sonnenberg, M. Hada, M. Ehara, K. Toyota, R. Fukuda, J. Hasegawa, M. Ishida, T. Nakajima, Y. Honda, O. Kitao, H. Nakai, T. Vreven, J. A. Montgomery, J. E. Peralta, F. OgliaroJr, M. Bearpark, J. J. Heyd, E. Brothers, K. N. Kudin, V. N. Staroverov, R. Kobayashi, J. Normand, K. Raghavachari, A. Rendell, J. C. Burant, S. S. Iyengar, J. Tomasi, M. Cossi, N. Rega, J. M. Millam, M. Klene, J. E. Knox, J. B. Cross, V. Bakken, C. Adamo, J. Jaramillo, R. Gomperts, R. E. Stratmann, O. Yazyev, A. J. Austin, R. Cammi, C. Pomelli, J. W. Ochterski, R. L. Martin, K. Morokuma, V. G. Zakrzewski, G. A. Voth, P. Salvador, J. J. Dannenberg, S. Dapprich, A. D. Daniels, O. Farkas, J. B. Foresman, J. V. Ortiz, J. Cioslowski and D. Fox, *Gaussian 09, Revision A.02*, Gaussian, Wallingford, 2009.

35 R. A. Kendall, T. H. Dunning and R. J. Harrison, *J. Chem. Phys.*, 1992, **96**, 6796–6806.

36 C. Lee, W. Yang and R. G. Parr, *Phys. Rev. B: Condens. Matter Mater. Phys.*, 1988, **37**, 785–789.

37 H. Chermette, *J. Comput. Chem.*, 1999, **20**, 129–154.

38 R. G. Parr, L. V. Szentpály and S. Liu, *J. Am. Chem. Soc.*, 1999, **121**, 1922–1924.

39 T. Le Bahers, C. Adamo and I. Ciofini, *J. Chem. Theory Comput.*, 2011, **7**, 2498–2506.

40 T. Lu and F. Chen, *J. Comput. Chem.*, 2012, **33**, 580–592.

41 M. Kamiya, H. Sekino, T. Tsuneda, K. Hirao and M. Kamiya, *J. Chem. Phys.*, 2005, **122**, 234111.

42 J. E. Rice, R. D. Amos, S. M. Colwell, N. C. Handy and J. Sanz, *J. Chem. Phys.*, 1990, **93**, 8828–8839.

43 R. Bersohn, P. A. O. Yoh-Han and H. L. Frisch, *J. Chem. Phys.*, 1966, **45**, 3184–3198.

44 A. Plaquet, M. Guillaume, B. Champagne, F. Castet, L. Ducasse, J. L. Pozzo and V. Rodriguez, *Phys. Chem. Chem. Phys.*, 2008, **10**, 6223–6232.

45 F. Castet, E. Bogdan, A. Plaquet, L. Ducasse, B. Champagne and V. Rodriguez, *J. Chem. Phys.*, 2012, **136**, 24506–24515.

46 H. Louis, I. B. Onyebuonyi, J. O. Odey, A. T. Igbalagh, M. T. Mbonu, E. A. Eno, A. M. S. Pembere and O. E. Offiong, *RSC Adv.*, 2021, **11**, 28433–28446.



47 P. S. V. Kumar, V. Raghavendra and V. Subramanian, *J. Chem. Sci.*, 2016, **128**, 1527–1536.

48 D. Paul, J. Deb and U. Sarkar, *ChemistrySelect*, 2020, **5**, 6987–6999.

49 E. Espinosa, I. Alkorta, J. Elguero and E. Molins, *J. Chem. Phys.*, 2002, **117**, 5529.

50 C. F. G. E. J. Baerends, T. Ziegler, A. J. Atkins, J. Autschbach, D. Bashford, A. Bérbes, F. M. Bickelhaupt, C. Bo, P. M. Boerriger, L. Cavallo, D. P. Chong, D. V. Chulhai, L. Deng, R. M. Dickson, J. M. Dieterich, D. E. Ellis, M. van Faassen, L. Fan and T. H. Fischer, ADF2016.01, SCM, Theor. Chem. Vrije Univ. Amsterdam, Netherlands, 2016, <https://www.scm.com>.

51 G. Te Velde, F. M. Bickelhaupt, E. J. Baerends, C. Fonseca Guerra, S. J. A. Van Gisbergen, J. G. Snijders and T. Ziegler, *J. Comput. Chem.*, 2001, **22**, 931–967.

52 M. Palusiak and T. M. Krygowski, *Chem. – Eur. J.*, 2007, **13**, 7996–8006.

53 E. Arunan, G. R. Desiraju, R. A. Klein, J. Sadlej, S. Scheiner, I. Alkorta, D. C. Clary, R. H. Crabtree, J. J. Dannenberger, P. Hobza, H. G. Kjaergaard, A. C. Legon, B. Mennucci and D. J. Nesbitt, *Pure Appl. Chem.*, 2011, **83**, 1637–1641.

54 P. R. Schleyer, C. Maerker, A. Dransfeld, H. Jiao, N. J. R. V. E. Hommes, D. Erlangen and R. V. February, *Am. Chem. Soc.*, 1996, **118**, 6317–6318.

55 P. R. Schleyer, B. Kiran, D. V. Simion and T. S. Sorensen, *J. Am. Chem. Soc.*, 2000, **122**, 510–513.

56 D. Hannachi, N. E. H. Amrane, L. Merzoud and H. Chermette, *New J. Chem.*, 2021, **45**, 13451–13462.

57 J. Li and A. Y. Rogachev, *Phys. Chem. Chem. Phys.*, 2016, 11781–11791.

58 A. Ayadi, L. Mydlova, N. Zouari, M. Makowska-janusik, B. Sahraoui and A. El-ghayoury, *Opt. Mater.*, 2016, 1–9.

59 R. N. Butler and S. M. Johnston, *J. Chem. Soc. Perkin Trans. 1*, 1984, 2109–2116.

60 M. A. Al-Sheikh and M. H. Elnagdi, *Molecules*, 2009, **14**, 4406–4413.

61 S. M. Landge and I. Aprahamian, *J. Am. Chem. Soc.*, 2009, **131**, 18269–18271.

62 X. Su and I. Aprahamian, *Org. Lett.*, 2011, **13**, 30–33.

63 S. M. Landge, E. Tkatchouk, D. Benítez, D. A. Lanfranchi, M. Elhabiri, W. A. Goddard and I. Aprahamian, *J. Am. Chem. Soc.*, 2011, **133**, 9812–9823.

64 X. Su, M. Lökov, A. Kütt, I. Leito and I. Aprahamian, *Chem. Commun.*, 2012, **48**, 10490–10492.

65 C. Lu, B. Htan, S. Fu, C. Ma and Q. Gan, *Tetrahedron*, 2019, **75**, 4010–4016.

66 P. Gilli, V. Bertolasi, L. Pretto, V. Ferretti and G. Gilli, *J. Am. Chem. Soc.*, 2004, **126**, 3845–3855.

67 V. Bertolasi, P. Gilli, V. Ferretti and G. Gilli, *J. Am. Chem. Soc.*, 1991, **113**, 4917–4925.

68 G. Gilli, F. Bellucci, V. Ferretti and V. Bertolasi, *J. Am. Chem. Soc.*, 1989, **111**, 1023–1028.

69 E. Espinosa, E. Molins and C. Lecomte, *Chem. Phys. Lett.*, 1998, **285**, 170–173.

70 I. Mata, I. Alkorta, E. Espinosa and E. Molins, *Chem. Phys. Lett.*, 2011, **507**, 185–189.

71 L. J. Karas, P. R. Batista, R. V. Viesser, C. F. Tormena, R. Rittner and P. R. De Oliveira, *Phys. Chem. Chem. Phys.*, 2017, **19**, 16904–16913.

72 A. V. Afonin, A. V. Vashchenko and M. V. Sigalov, *Org. Biomol. Chem.*, 2016, **14**, 11199–11211.

73 L. R. Domingo, M. J. Aurell, P. Pérez and R. Contreras, *Tetrahedron*, 2002, **58**, 4417–4423.

74 L. Wang, J. Ye, H. Wang, H. Xie and Y. Qiu, *Sci. Rep.*, 2017, **7**, 1–11.

75 K. S. Thanthiriyawatte and K. M. Nalin de Silva, *THEOCHEM*, 2002, **617**, 169–175.

76 R. V. Solomon, P. Veerapandian, S. A. Vedha and P. Venuvanalingam, *J. Phys. Chem. A*, 2012, **116**, 4667–4677.

77 N. Hou, R. Feng and X.-H. Fang, *Int. J. Quantum Chem.*, 2022, **122**, 1–14.

78 J. L. Oudar and D. S. Chemla, *J. Chem. Phys.*, 1976, **66**, 2664–2668.

79 C. Tonnelé and F. Castet, *Photochem. Photobiol. Sci.*, 2019, **18**, 2759–2765.

80 M. Zhang, C. Wang, W. Wang, N. Ma, S. Sun and Y. Qiu, *J. Phys. Chem. A*, 2013, **117**, 12497–12510.

